DEGREE PROJECT IN TECHNOLOGY,
SECOND CYCLE, 30 CREDITS
STOCKHOLM, SWEDEN 2022

Topological Photonic Lattices

KTH Master Thesis Report

Zesheng Xu

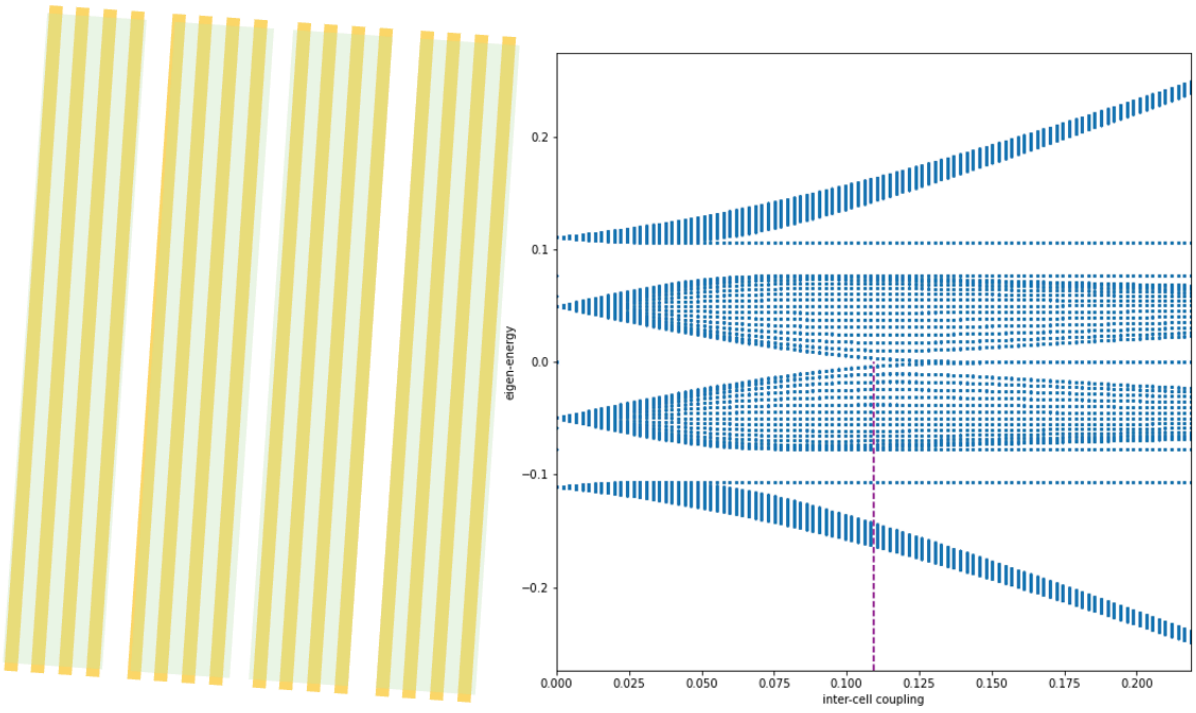

KTH ROYAL INSTITUTE OF TECHNOLOGY
Engineering Physics

Author

Zesheng Xu <zesheng@kth.se>
Applied Physics
KTH Royal Institute of Technology

Place for Project

Stockholm, Sweden
Quantum Nano photonics group-KTH

Examiner

Professor. Val Zwiller
KTH Royal Institute of Technology

Supervisor

Associate Professor. Ali Elshaari

KTH Royal Institute of Technology

Abstract

Topological Photonics is a rapidly growing field which explores the ideas of topological invariants adapted from condensed matter physics to optical systems. Thanks to integrated photonics platforms, the evolution of light in nanoscale photonic lattices can enable direct measurement of topological properties of the band-structure.

In this degree project, we study the topological Anderson phase transition in disordered one-dimensional lattices, and probe distinct topological phases in photonic superlattices. In first part, we fabricate photonic lattices with different disorder strength, and observe the topological transition from trivial topological Anderson phase to non-trivial topological Anderson phase as the system disorder is increased.

In second part, we focus on probing the Zak phase in photonic superlattices. We fabricate a superlattice system that utilizes either bulk excitation or edge excitation. We identify the trivial and non-trivial Zak phase using two methods: first, through reconstructing the intensity evolution in the edge waveguide, second, through calculating the beam displacement in the case of bulk excitation .

In order to study the evolution of the light in the nano-scaled photonic lattices, we develop a novel technique: Loss-Induced Scattering Approach (LISA), which enables high fidelity reconstruction of the photonic state evolving in the lattice.

Keywords

Topological photonics, Integrated photonics, Condensed matter physics physics, Optics

Abstract

Topologisk fotonik är ett snabbt växande område som utforskar idéerna om topologiska invarianter anpassade från kondenserad materiens fysik till optiska system. Tack vare integrerade fotonikplattformar kan ljusutvecklingen i fotoniska gitter i nanoskala möjliggöra direkt mätning av topologiska egenskaper hos bandstrukturen.

I detta examensarbete studerar vi den topologiska Anderson-fasövergången i oordnade endimensionella gitter, och undersöker distinkta topologiska faser i fotoniska supergitter. I den första delen tillverkar vi fotoniska gitter med olika störningsstyrka och observerar den topologiska övergången från trivial topologisk Anderson-fas till icke-trivial topologisk Anderson-fas när systemstörningen ökar.

I den andra delen fokuserar vi på att sondera Zak-fasen i fotoniska supergitter. Vi tillverkar ett supergittersystem som använder antingen bulkexcitering eller kantexcitering. Vi identifierar den triviala och icke-triviala Zak-fasen med två metoder: för det första genom att rekonstruera intensitetsutvecklingen i kantvågledaren, för det andra genom att beräkna strålens förskjutning vid bulkexcitation.

För att studera utvecklingen av ljuset i de nanoskalade fotoniska gittren, utvecklar vi en ny teknik: Loss-Induced Scattering Approach (LISA), som möjliggör högtrohetsrekonstruktion av det fotoniska tillståndet som utvecklas i gittret.

Nyckelord

Topologisk fotonik, Integrerad fotonik, Kondenserad materiens fysik, Optik

Acknowledgements

First of all I would like to thank my supervisor Associate Professor Dr. Ali Elshaari for his kind guidance and profound knowledge. He is always open to discuss physics background and technology details. What's more, he often offered heuristic advice when I face difficulties. This project would not have been carried on without his inputs and enthusiasm.

Then I want to thank my senior fellow apprentice Dr. Jun Gao for his guidance in experimental and computer skills patiently. At the beginning of this project, both computer simulation and experimental measurements were challenging for me. However, under his systematic training, I can now write simulation codes and perform topological photonics experiments independently.

Furthermore I want to thank the group leader Professor Dr. Val Zwiller. He arranged the lab with top equipments. Prof. Zwiller not only has a very wide view of the history of quantum photonics, but it is coupled with a keen sense technological potential for the fundamental physics experiments we perform in the lab.

I would like to thank Dr. Stephan Steinhauer and Ph.D. student Govind Krishna for their contribution in the fabrication of the chips. Their effort and excellent developed fabrication process made the results possible. I also want to thank all other members in QNP group for their help and a very pleasant atmosphere.

Finally I want to thank my parents for their financial and emotional Support. Their honest and hardworking attitude always encourage me to explore the boundless sea of truth bravely.

Contents

Chapter 1

Introduction

The field of topological photonics focuses on exploring the parallels between topological invariants in condensed matter systems with the optical ones, and utilize their properties to build advanced photonic devices. Topological phases of matter were initially explored in solid-state electroninc systems, such as the integer quantum Hall effect discovered in 1980[1]. In 2008, Haldane and Raghu showed that the photonics bands would have non-trivial topological invariants when the electromagnetic waves are guided in two-dimensional spatially periodic devices with time-reversal symmetry breaking using magneto-optical elements[2]. One year later, Wang experimentally implemented this idea in the microwave domain and measured the nontrivial band[3]. These works lead to numerous subsequent experiments in the following years. By carefully designing the wavevector space of the photonic lattice, a photonic system can allow light to propagate robustly against imperfections and disorder, with negligible back-reflection.

Topological photonics is not only an excellent platform for implementing theoretical concepts from condensed matter physics, but also has great technological importance with potential to create novel devices in the field of quantum photonics[4], non-linear photonics[5], on-chip robust communication and topologically protected lasers[6]. In this project, we focus on the investigation of two important topological concepts, -Anderson phase transition and Zak phase in a topologically protected band structure.

This report is divided to the following main parts, with brief summary presented below for each chapter:

Chapter 2, *Theoretical Background*, introduces the theoretical concepts and relevant formulas to study the photonic lattices.

Chapter 3, *Simulation and Chip design*, presents the simulation performed to study the light dynamics in the topological Anderson phase transition lattice, and the superlattice.

Chapter 4, *Sample Fabrication*, introduces the techniques used to fabricate the photonic chips.

Chapter 5, *Experimental Setup*, introduces the methods and experimental details for measuring the devices.

Chapter 6, *Data analysing*, analyse the measured data, with comparison to the simulation results.

Chapter 7, *Conclusion and Future outlook*, sums up the results we obtained and explore subsequent experiments in the waveguides array systems.

Chapter 2

Theoretical Background

2.1 Topology

Some topological properties of closed manifolds are preserved under continuous deformation, and only changed when opening or closing a hole in the manifold, which results in the increasing or decreasing of genus. For example, while kneading the dough into a pizza, the original dough and the resulting pizza are topologically equivalent even if the shape looks different. The reason is that in the process of making the pizza no new holes were introduced and the genus of these two geometric objects stays zero. However, if we are going to make some donuts, the change in topology is unavoidable. Different topologies can be mathematically characterized by topological invariants. When a hole is created or annihilated, the topological invariant changes and refers to a topological phase transition.

Topologies in photonics are defined on the dispersion bands in wave-vector space. In particular, we use Chern number to represent the topological invariant of 2D dispersion band. The Chern number can be calculated through integrating the curvature in k-space over the Brillouin zone.

$$C_m = \frac{1}{2\pi} \int_{BZ} \Omega_m(\mathbf{k}) \cdot d^2\mathbf{k} \tag{2.1}$$

where m is the band index, $\Omega_m(\mathbf{k})$ is the Berry curvature and $d^2\mathbf{k}$ is the small area in the reciprocal-space.

In 2D dispersion band, this represents the flux of Berry curvature through the

Figure 2.1.1: **Left:** Dough and pizza with same genus=0 **Right:** Dough and donuts with different genus

surface, and the chern number is always an integer. This integer characterizes the quantized collective behaviour of the wavefunctions on the band. If an observable described by a topological invariant, it can only change discretely and would not react to small continuous perturbations, which results in the natural robustness against imperfections.

To illustrate it, we first go through the definition of Berry curvature.

$$\mathbf{\Omega}_m(\mathbf{k}) = \nabla_{\mathbf{k}} \times \mathcal{A}_m(\mathbf{k}) \tag{2.2}$$

and $\mathcal{A}_m(\mathbf{k})$ is the Berry connection defined by the following formula:

$$\mathcal{A}_m(\mathbf{k}) = i \left\langle u_{m\mathbf{k}} \left| \nabla_{\mathbf{k}} \right| u_{m\mathbf{k}} \right\rangle \tag{2.3}$$

where $u_{m\mathbf{k}}$ is the spatially periodic part of the Bloch function.

2.2 Photonic waveguides

The evanescently coupled photonic waveguides shown in the figure 2.2.1 is an excellent platform for studying discrete systems.

We can compare the Schrödinger equation of this 2D system and the optical paraxial Helmholtz equation for the evolution of the amplitude of the electrical field.

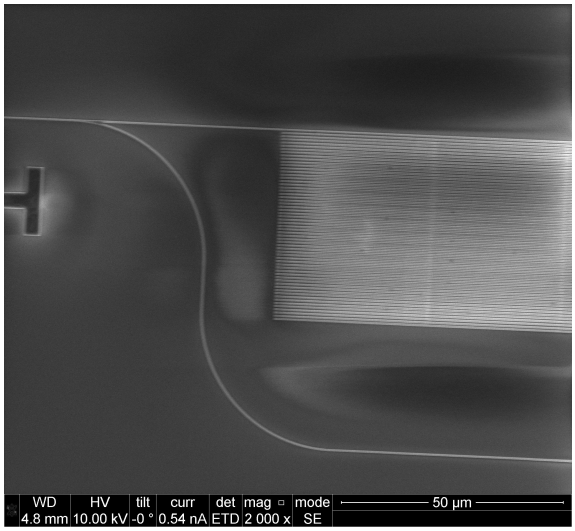

Figure 2.2.1: **SEM image of superlattice photonics array**

$$-\frac{\overline{h}^2}{2m}\nabla^2\Psi(x,t)+V(x,t)\Psi(x,t)=i\overline{h}\frac{\partial}{\partial t}\Psi(x,t) \tag{2.4}$$

and

$$\mathrm{i}\lambda\frac{\partial}{\partial z}E(x,z)=(-\frac{\lambda^2}{2n_0}\frac{\partial^2}{\partial x^2}+\Delta n(x,z))E(x,z) \tag{2.5}$$

These two equations have analogous character due to the corresponding relationship between t and z, $\overline{h}$ and $\lambda = \lambda/2\pi$, m and waveguides refractive index n_0, V and refractive index change$\Delta n = n_0 - n(x,z)$. It shows that in the photonics system the evolution of the wave packet takes place in space, compared to time in the Schrödinger equation for electrons. This photonic platform allows us to study the time-dependent equations in the models introduced by condensed matter physics and their properties by directly observing the light propagation in a simple photonic chip in a very small time scale.

2.3 Topological Anderson phase

2.3.1 SSH model

Su-Schreifer-Heeger(SSH) model as the figure 2.3.1 shows is the simplest one-dimensional model to identify trivial and non-trivial phases. We can characterize these two phases with winding number W, which is tuned by controlling the relation between

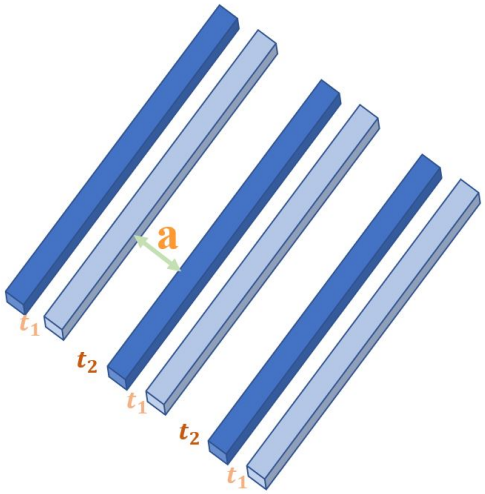

Figure 2.3.1: **Schematic of an SSH lattice:**
The light blue and dark blue waveguides represent the different atoms in SSH model, each two atoms form a unit cell, t_1 and t_2 are the intra-cell and inter-cell coupling strength. The periodic distance between cells is a

the intra/inter-cell coupling amplitudes t_1/t_2.

To analyse this model, we introduce tight-binding approximation which only considers the coupling between the nearest neighboring atoms. We start with the Hamiltonian of a single electron in atomic chain:

$$H = \frac{p^2}{2m} + U(x) \tag{2.6}$$

with periodical potential:

$$U(x + na) = U(x) \tag{2.7}$$

Assume the potential energy term of a single atom to be $V(x)$:

$$H_0 = \frac{p^2}{2m} + V(x) \tag{2.8}$$

with time-independent Schrödinger equation:

$$H_0\phi(x) = E_0\phi(x) \tag{2.9}$$

Then we get the total wave function to be a linear combination of wave functions at

different lattice sites:

$$\psi(x) = \sum_n a_n \phi_n \tag{2.10}$$

We note that $\phi_n = \phi\left(x - x_n\right), x_n = na$ and define $\Delta U(x) = U(x) - V(x)$ we get:

$$\sum_n \left\langle \phi_m \left| \Delta U\left(x - x_n\right) \right| \phi_n \right\rangle a_n = \left(E - E_0\right) a_m \tag{2.11}$$

We now define

$$\langle \phi(x - ma + na) | \Delta U(x) | \phi(x) \rangle = -J\left(x_m - x_n\right) \tag{2.12}$$

and get:

$$-\sum_n J\left(x_m - x_n\right) a_n = \left(E - E_0\right) a_m \tag{2.13}$$

Using bloch formalism, we would have:

$$E - E_0 = -\sum_n J\left(x_n\right) e^{-ikx_n} \tag{2.14}$$

Consider the nearest neighbors coupling, which means we only care about the position $-a$,0, and $+a$, we can have the simplified formula foe the dispersion relation:

$$E - E_0 + J_0 = -J(e^{ika} + e^{-ika}) = -2J \cos ka \tag{2.15}$$

$$E - E_0 = -J_0 - J(e^{ika} + e^{-ika}) = -2J \cos ka \tag{2.16}$$

From the second quantization view, we can write the Hamiltonian into the matrix language:

$$H = \langle \psi | H | \psi \rangle \Rightarrow \hat{H} = \sum_{m,n} \hat{c}_m^\dagger H_{mn} \hat{c}_n \tag{2.17}$$

With tight-binding approximation we only consider the nearest coupling and have:

$$\hat{H} = \sum_{n=1}^{M} \hat{c}_n^{\dagger} \hat{c}_{n+1} t_n + h.c. \tag{2.18}$$

where $\hat{c}_n^{\dagger}(\hat{c}_n)$ and $\hat{c}_{n+1}^{\dagger}(\hat{c}_{n+1})$ are the creation (annihilation) operators for two atoms in one single unit cell.

2.3.2 Energy band and Winding number

Energy band

We can rewrite Hamiltonian through defining two local lattice sites in the figure 2.3.1, dark blue a_n, and the light blue as b_n, both located in the n_{th} cell, we have:

$$H = \sum_{n} \left(t_1 a_n^{\dagger} b_n + t_2 b_n^{\dagger} a_{n+1} \right) + h.c. \tag{2.19}$$

By solving equation:

$$\hat{\mathrm{H}} |\Psi\rangle = E |\Psi\rangle \tag{2.20}$$

we get the eigen-energy (assuming periodic of the system a=1):

$$E(k) = \pm \sqrt{t_1^2 + t_2^2 + 2 t_1 t_2 \cos(k)} \tag{2.21}$$

Winding number

Winding number of a closed curve in the plane around a fixed point is an integer, which represents the total number of times that the curve winds around the point.

We can rewrite the Hamiltonian in the Pauli matrix basis:

$$H(k) = \mathbf{h}(k) \cdot \sigma \tag{2.22}$$

and define the winding number W as:

$$W = \frac{1}{2\pi i} \int_{-\pi}^{\pi} dk \frac{d}{dk} \ln(h(k)) \tag{2.23}$$

In our SSH model, for $W = 1, t_1 < t_2$, this chain shows topological nontrivial phase; on the other hand for $W = 0, t_1 > t_2$, the chain shows topological trivial phase.

2.3.3 Anderson localization

Anderson localization is the absence of transport of waves in a disordered system[7]. By introducing the disorder V into tight-binding model:

$$\begin{aligned} & i\overline{h}\frac{d\psi}{dt} = H\psi \\ & H\psi_j = E_j\psi_j + \sum_{k\neq j} V_{kj}\psi_j \\ & V(|r|) = \begin{cases} 1, & |r| = |j-k| = 1 \\ 0, & \text{otherwise.} \end{cases} \end{aligned} \tag{2.24}$$

In 1d or 2d systems, the probability distribution remains localized uniformly in time t:

$$\sum_{n\in\mathbb{Z}^d} |\psi(t,n)|^2 |n| \leq C \tag{2.25}$$

where C represents a constant. This phenomenon is the famous Anderson localization.

Tal Schwartz firstly observed the Anderson localization[8] in disordered two-dimensional photonic lattices as shown in the figure 2.3.2 .

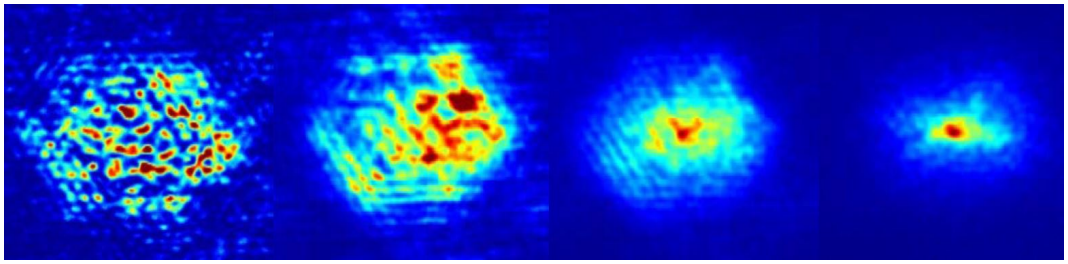

Figure 2.3.2
Facet image of light intensity localization in disordered 2d photonic lattices: From left to right: clear lattice, 0.025 disorder, 0.15 disorder, 0.45 disorder

2.3.4 Anderson phase transition

For a long time, it was believed that if disorder is introduced into a condensed matter system, a topological non-trivial phase would turn into a trivial phase due

to the influence of Anderson localization. However, recently it was showed that adding disorder to the trivial band structure would lead to a phase transition to the non-trivial phase[9], this phenomenon is referred to as topological Anderson phase transition.

2.4 Superlattice and Zak phase

2.4.1 Superlattice

The superlattice is a periodic structure of sites of two or more materials which was discovered in 1925 by Johansson and Linde[10]. They studied the gold-copper and palladium-copper systems through their X-ray diffraction patterns. Particularly, in this project we focus on periodic waveguide arrays with superlattice characteristics. The structure we choose is shown in the figure 2.4.1. In this model t_1, t_2, t_3 refer to the intra-cell coupling strength between the waveguides in tight-binding approximation, and $\mathcal{T}$ is the inter-cell coupling strength. The Hamiltonian of this system is[11]:

$$\hat{H} = \sum_{n=1}^{15} \left\{ \left(\sum_{l=1}^{3} t_l \hat{a}_{n,l}^{\dagger} \hat{a}_{n,l+1} \right) + \tau \hat{a}_{n,M}^{\dagger} \hat{a}_{n+1,1} + H.c. \right\} \tag{2.26}$$

where $\hat{a}_{n,l}^{\dagger}(a_{n,l}^{\dagger})$ is the photon creation (annihilation) operator at the (n,l)-th waveguide.

Rewrite the Hamiltonian in momentum space with matrix formalism:

$$\mathcal{H}_{n,m}(k) = t_n \delta_{n,m-1} + t_m \delta_{n,m+1} + \tau \exp(-ik)\delta_{n,1}\delta_{m,3} + \tau \exp(ik)\delta_{n,3}\delta_{m,1} \tag{2.27}$$

where k is the wave number in Bloch space and varies between $(-\pi, \pi)$. The energy bands $E_l(k)$ and the Bloch functions $u_l(k)$ are defined as:

$$\begin{aligned} \mathcal{H}(k)u_l(k) &= E_l(k)u_l(k) \\ \langle u_l(k) \mid u_n(k) \rangle &= \delta_{n,l} \end{aligned} \tag{2.28}$$

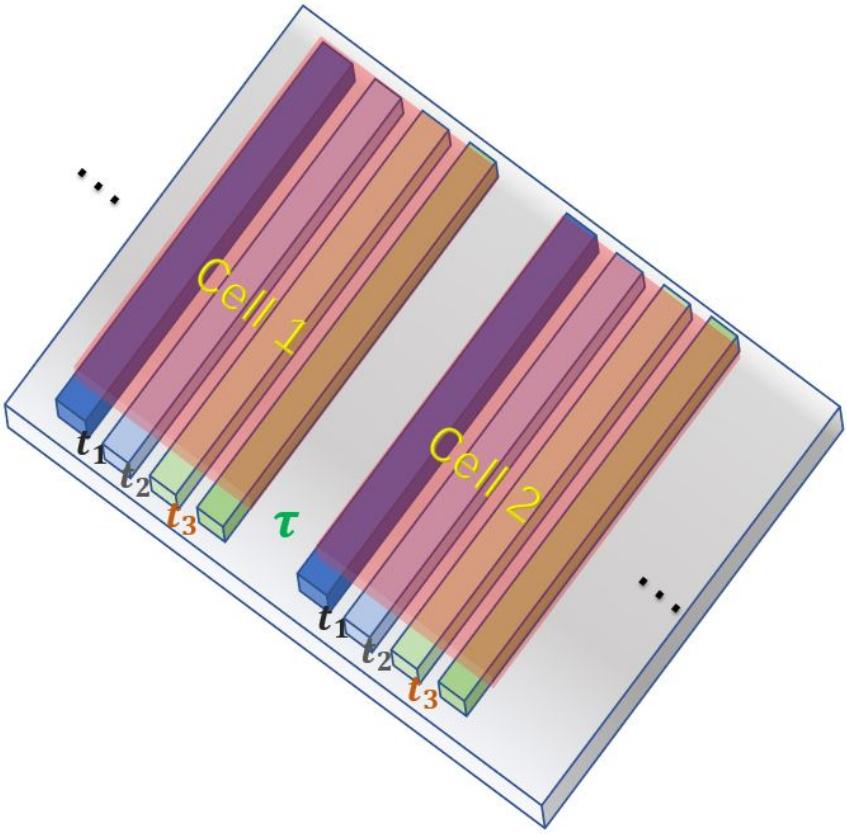

Figure 2.4.1
Schematic of the photonic superlattice The superlattice contains 15 cells, and each cell contains 4 equal waveguides. The waveguides are integrated in a substrate.

2.4.2 Probing Zak phase

Zak phase

The Zak phase is calculated by integrating the Berry connection $\mathcal{A}_l(\mathbf{k}) = i\langle u_l(\mathbf{k})|\nabla_{\mathbf{k}}|u_l(\mathbf{k})\rangle$ along one single wave vector axis, which was introduces by J.Zak in 1989[12]. The Zak phase is then the one dimensional special case of the Berry phase that we explored earlier in this report. The Zak phase for the $l-th$ band reads:

$$\gamma_l = i\int_{-\pi}^{\pi} dk\,\langle u_l(k)\mid (du_l/dk)\rangle \tag{2.29}$$

In our superlattice model shown in figure 2.4.1, we have M=4 sites result in S=3 band gaps in between under tight-binding approximation. The topological nature of these 3

band gaps is attributed by the Zak phases sum.

$$\mathcal{N}_n = \gamma_1 + \gamma_2 + \gamma_3 \tag{2.30}$$

Wannier functions are a complete set of orthogonal functions used in solid-state physics. The most widely used Wannier function is defined according to the Bloch states $\psi_{\mathbf{k}}(\mathbf{r}) = e^{i\mathbf{k}\cdot\mathbf{r}}u_{\mathbf{k}}(\mathbf{r})$, where $u_{\mathbf{k}}(\mathbf{r})$ denotes the periodicity in lattice. Then the Wannier function reads:

$$\phi_{\mathbf{R}}(\mathbf{r}) = \frac{1}{\sqrt{N}}\sum_{\mathbf{k}} e^{-i\mathbf{k}\cdot\mathbf{R}}\psi_{\mathbf{k}}(\mathbf{r}) \tag{2.31}$$

If we excite the $n-th$ site of a superlattice, we reproduce the Wannier function of the $n-th$ band and result in a shift of the total Wannier function[13]. The topology of Zak phase originates from this shift of the Wannier band, with only two absolute values allowed.

$$|\gamma_l| = \begin{cases} 0, \text{topological trivial phase} \\ \pi, \text{topological non-trivial phase} \end{cases} \tag{2.32}$$

Displacement

In a recent work it was shown theritically that the average beam displacement in a two-band photonic lattice can reveal the Zak phase[14]. In 2019, Longhi proposed that we can use this idea also in the multi-gap superlattice systems[11]. Particularly speaking, we take $M = 4$ in each cell and the propagation of the electromagnetic field amplitudes can be written as the superposition of Bloch modes:

$$a_n(z) = \sum_{l=1}^{4}\int_{-\pi}^{\pi} dk C_l(k)u_l(k)\exp\left[ikn - iE_l(k)z\right] \tag{2.33}$$

where the spectral amplitudes are decided by the initial excitation states and the normalization condition:

$$
\begin{aligned}
C_l(k) &= (1/2\pi)\sum_n \langle u_l(k) \mid a_n(0)\rangle \exp(-ikn) \\
2\pi &\sum_l \int_{-\pi}^{\pi} dk\, |C_l(k)|^2 = 1
\end{aligned}
\tag{2.34}
$$

The beam displacement along the propagation distance z reads:

$$
\mathcal{D}(z) = (1/z)\int_0^z d\xi \sum_{n=-\infty}^{\infty} n \langle a_n(\xi) \mid a_n(\xi)\rangle \tag{2.35}
$$

It is important that the displacement is a directly measurable quantity. In large z limit the displacement reaches a asymptotic form:

$$
\mathcal{D}_{\text{as}} = 2\pi i \sum_{l=1}^{M} \int_{-\pi}^{\pi} \mathrm{d}k \left(C_l^*(k)\frac{dC_l}{dk} + |C_l(k)|^2 \left\langle u_l(k) \mid \frac{du_l}{dk} \right\rangle \right) \tag{2.36}
$$

When we excite the lowest bands with number S of the superlatice and assuming $C_l(k) = 1/(2\sqrt{S}\pi)$ for normalization which is independent of k, we can get the interesting and simple equation:

$$
\mathcal{D}_{\text{as}} = (1/2\pi S)\sum_{l=1}^{S} \gamma_l = \mathcal{N}_S/(2\pi S) \tag{2.37}
$$

For our $M = 4$ model, if we use single-cell excitation with the initial condition:

$$
a_n = (1/\sqrt{2})(1, 0, e^{i\theta}, 0)^T \delta_{n,0} \tag{2.38}
$$

where the relative phase shift θ is chosen in the range of $(-\pi, +\pi)$. Intuitively speaking, only two waveguides of the array separated by two sites are equally excited at the input plane. From theoretical prediction, we have the following relationship:

$$
\mathcal{D}_{as} = \begin{cases} 0, \text{ for } \tau < \tau_0 \\ -0.25, \text{ for } \tau > \tau_0 \end{cases} \tag{2.39}
$$

where $\tau_0 = t_1 t_3/t_2$. Now our aim is designing a chip and a experiment to verify it.

Chapter 3

Simulation

3.1 Topological Anderson phase

We simulate a photonic waveguides array comprising 50 sites, with intra-cell coupling strength $t_1 = 0.0126$ and the inter-cell coupling strength $t_2 = 0.063$. The figure 3.1.1 shows the model of a simple SSH lattice. For $t_1 > t_2$, the system has a topological trivial band structure with a non-zero winding number, and $t_2 > t_1$ for non-trivial band structure with a zero winding number. The light propagation in the waveguide array can be described by the following coupled-mode equations:

$$\begin{aligned} i\frac{da_n}{dz} &= t_1 b_n + t_2 b_{n-1} \\ i\frac{db_n}{dz} &= t_1 a_n + t_2 + V_n a_{n+1} \end{aligned} \tag{3.1}$$

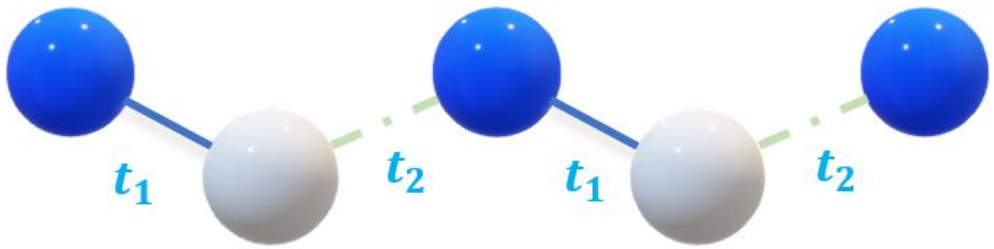

Figure 3.1.1: **A schematic of SSH model**

Then we add incommensurate disorder in the inter-dimer bonds as V_n for the nth cell

as shown in figure 3.1.2. The coupled-mode equations for the disordered system can be rewritten as:

$$\begin{aligned} i\frac{da_n}{dz} &= t_1 b_n + (t_2 + V_{n-1})\, b_{n-1} \\ i\frac{db_n}{dz} &= t_1 a_n + (t_2 + V_n)\, a_{n+1} \end{aligned} \tag{3.2}$$

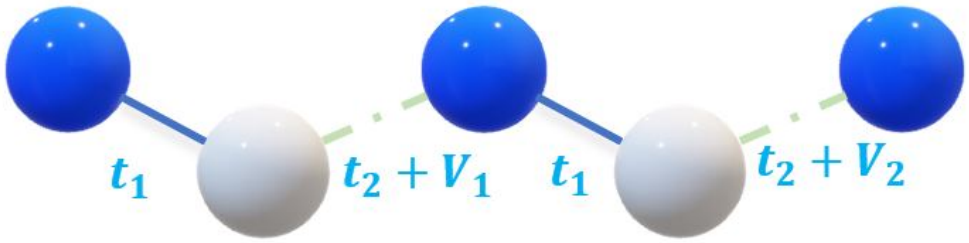

Figure 3.1.2: **A schematic of incommensurately disordered SSH model**

We add a disorder of $V_n = Vcos(2\pi\alpha n)$ to the inter-cell coupling strength t_2, and assume α to be an irrational number, selected here to be a Fibonacci number $\alpha = q_n = (\sqrt{5}-1)/2$. In this disordered system we can numerically calculate a generalized winding number Q with disorder strength $\frac{V}{t_1}$ in the range of $(0, 4)$. The generalized winding number Q can be written as[15]:

$$Q = \frac{1}{2}\left(1 - \text{sign}\left\{\prod_n t_1^2 - \prod_n (t_2 + V_n)^2\right\}\right) \tag{3.3}$$

Figure 3.1.3 is the simulation result for a 50 sites lattice:

We introduce the concept of inverse participation ratio (IPR), which was proposed by G. Corrielli in 2013[16], to study the localization of beam in different eigen states:

$$I_l = \frac{\sum_n \left(\left|a_n^{(l)}\right|^4 + \left|b_n^{(l)}\right|^4\right)}{\left(\sum_n \left(\left|a_n^{(l)}\right|^2 + \left|b_n^{(l)}\right|^2\right)\right)^2} \tag{3.4}$$

The figure 3.1.4 shows the numerically computed IPR values versus the disorder strength in range of $(0, 4)$. To give a more details about the system behaviour, we choose

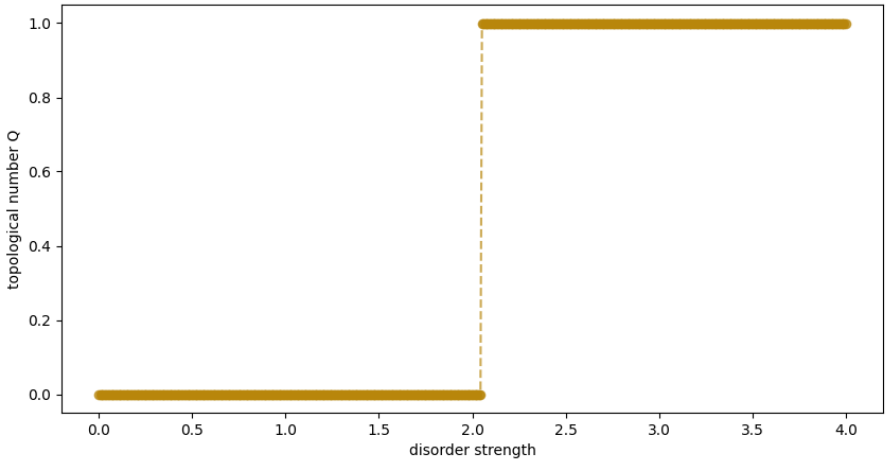

Figure 3.1.3: **Topological number Q for a SSH lattice with 50 sites versus disorder strength** V/t_1 The topological transition point is $V/t_1 = 2$ as the dashed line indicates, from trivial winding number 0 to non-trivial winding number 1

500 lattice sites rather than 50 to approach the infinite chain approximation. The IPR plot is a good criterion to predict the light evolution in SSH lattices with different disorder strengths, providing a guideline before perfomring the experiment.

After the calculation of the IPR values, we choose four typical disorder strength $V_1 = 0$, $V_2 = 0.2t_1$, $V_3 = t_1$ and $V_4 = 2.5t_1$ to simulate the light dynamics for single site excitation of the left edge. Traditionally, the localization of the light was used to infer the topological phase of the system. For a disorder-free SSH lattice, the topological phase $Q = 0$ corresponds to a non-localized edge state while $Q = 1$ corresponds to a localized edge state. However, figure 3.1.5 indicates that it is difficult to distinguish the topological Anderson phase in cases c) and d) by simply observing the light dynamics due to the rapid localization as the disorder strength is increased above the critical point $V = 2t_1$.

To overcome this difficulty we introduce the spectral method[17] to probe the topological Anderson phase by measuring the light dynamics at the edge waveguide of the photonic SSH lattice. We set $a_1(z)$ as the amplitude of the light in edge site, and the initial state reads:

$$(a_n, b_n) = (1, 0)^T \delta_{n,1} \tag{3.5}$$

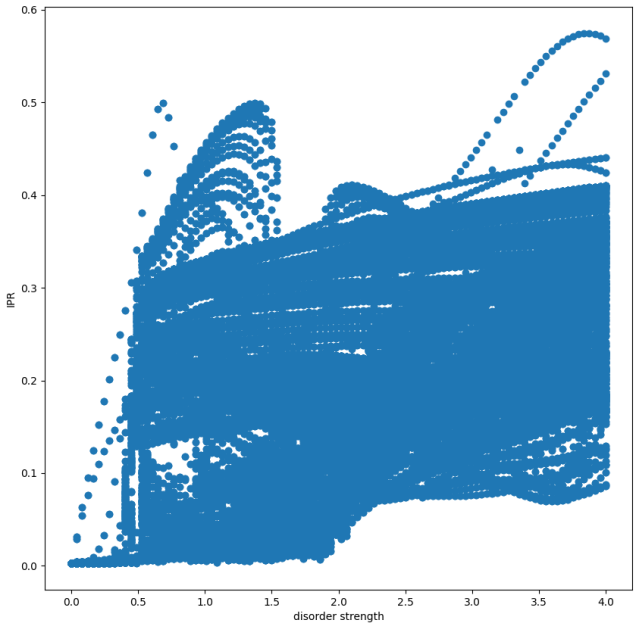

Figure 3.1.4: **Inverse participation ratio (IPR) versus disorder strength** The zero IPR value refers to full delocalization, and the non-zero IPR values refer to the localization. From left to right, we can find that in disorder range (0,0.5), most of the eigen states are delocalized, in range (0.5, 2) it is a mixture state with delocalization and localization. When the disorder strength $V > 2t_1$, the eigen states are fully localized, which implies the localization of the light intensity in edge site along the propagation distance.

Consider the definition of the correlation function:

$$C(E) = \frac{1}{L}\int_0^L dz a_1^*(0)a_1(z)\exp(iEz) \tag{3.6}$$

where L is the propagation distance. In our single waveguide excitation used in the experiment $a_1(0) = 1$, so this equation reduces to the Fourier transform:

$$C(E) = \frac{1}{L}\int_0^L dz a_1(z)\exp(iEz) \tag{3.7}$$

Rewrite this equation in the following form[18]:

$$C(E) = \sum_l \alpha_l[\sin((E - E_l)L/2)]^2/((E - E_l)L/2)^2 \tag{3.8}$$

where α_l refers to the spectral weight of the initial edge excitation into the lth eigen

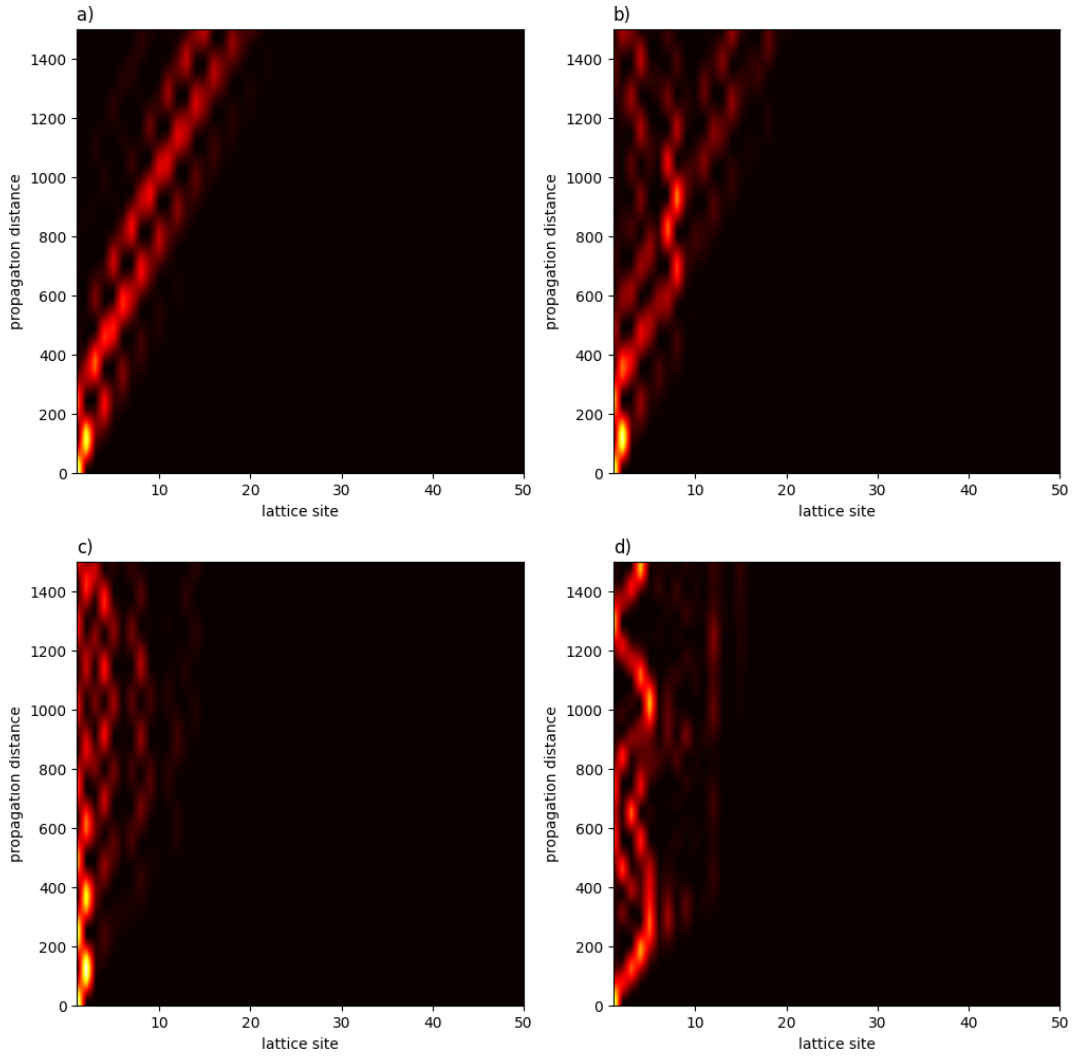

Figure 3.1.5: **Light dynamics in SSH lattice with different disorder strengths** a) $V = 0$ b) $V = 0.2t_1$ c) $V = t_1$ d) $V = 2.5t_1$ From a) to d) it clearly shows the counter-intuitive result that the light is more localized in the edge as the disorder strength is rising

mode with energy E_l. We can reconstruct the correlation function by measuring the evolution of light intensity in the edge waveguide and taking the square root to rebuild the amplitudes. With the amplitudes and eq3.8, it is enough to trace the correlation function $C(E)$ and thereby probe the topological Anderson phase. For example, we reconstruct the Anderson phases of the lower two images we mentioned before in 3.1.5. The following figure3.1.6 shows the numerically computed correlation function C_E for $V = t_1$ and $V = 2.5t_1$ respectively. From top to bottom, we firstly draw the light evolution patterns along the propagation distance, then we calculated the light intensity in the left-edge waveguide, and retrieve the amplitude by taking the square root. Finally we draw the correlation function with the simulated data. It is obvious that even if there are two cases were the light is localized within two disorder strengths,

we can distinguish their topological Anderson phase effectively by identifying whether these is a zero-energy peak in the correlation function spectrum. The zero-energy peak exists when the topological number $Q = 1$, which corresponds to the topological non-trivial phase, while the zero-energy disappears when the topological number $Q = 0$, corresponding to the topological trivial phase. Our goal is to perform the experimental measurement for the light intensity in the left-edge waveguide along the propagation distance and then retrieve the correlation function C_E.

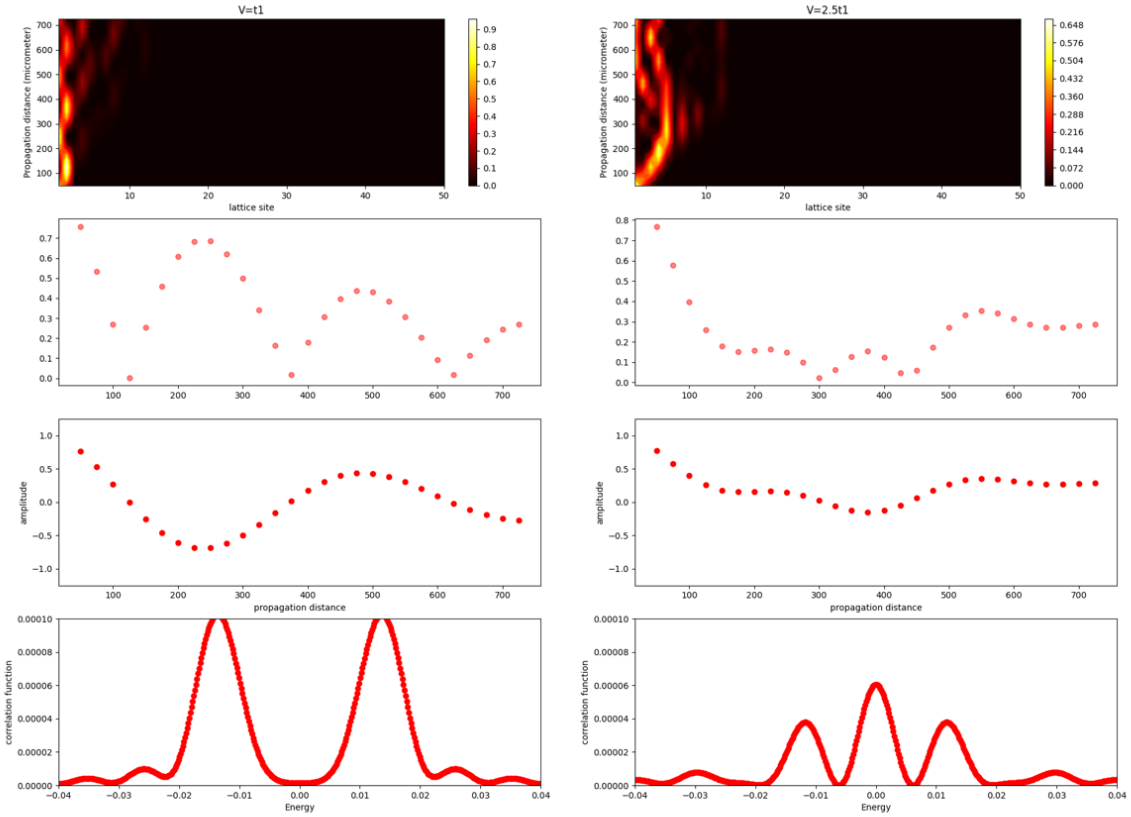

Figure 3.1.6: **Numerically computed correlation function** C_E From top to bottom, we draw the patterns of simulated light dynamics, monitor the light intensity, retrieve the light amplitude, and reconstruct the correlation function. The criterion to characterize the topological number and the Anderson phase is whether these exists a zero-energy peak in the spectrum. The left one refers to a topological trivial phase without a zero-energy peak, and the right one refers to a topological non-trivial phase with a zero-energy peak. The result is accord with our previous assumption.

3.2 Topological Superlattice

In the superlattice described in the previous chapter, we set $t_1 = 0.0587$, $t_2 = 0.0503$, $t_3 = 0.0902$, $\tau_1 = 0.052$, $\tau_2 = 0.194$, $M = 4$, $N = 15$. t_{1-3} are the intra-cell coupling strengths,while $\tau_1 < \tau_0 = t_1 t_3/t_2$ and $\tau_2 > \tau_0 = t_1 t_3/t_2$ are the topological trivial/non-trivial inter-cell coupling strengths. M indicates the number of waveguides in each cell, while N refers to the total cell number. By constructing the matrix Hamiltonian and the time-evolution operator e^{-iHt}, we can now numerically investigate the light dynamics in topological photonic lattices before the chip design. This simulation helps us choose the appropriate fabricated chip parameters.

The figure 3.2.1 shows the eigen energy spectrum corresponds to the superlattice we introduced before without inversion symmetry. The top and bottom bands emanate away as the inter-cell coupling is increasing without closing, which indicates that these two bands are not are topological trivial.The middle band gap is closing and reopening at $\tau_0 = t_1 t_3/t_2$. This zero-energy degenerate state implies the sudden topological transition of Zak phase $\mathcal{N}_2$ from 0 (trivial) to π (non-trivial).

We firstly excite the superlattice array in the edge as the fig 3.2.2 shows. The left panel shows the light evolution as it propagates in topological non-trivial (a)/trivial superlattice (c). It is obvious that in the upper part the light is mostly localized in the edge waveguide after long propagation distance, with another intensity peak that moves from left to right in the range of the diffusion length of the system. However, as the right panel shows, the light intensity in the edge waveguide of the non-trivial case oscillates, which makes it difficult to discriminate the non-trivial zero-energy mode from the trivial ones. Especially in experiment, as it is much more challenging to identify the two phases with edge excitation alone. In other words, it challenging to quantify the degree of "oscillation" as a measure of the topological phase.

As a solution to challenges of edge excitation, we consider the single cell bulk excitation presented by Longhi[11]. We inject the laser in the first and the third waveguide in one cell with phase difference π, and the initial state can be written as:

$$a_n = (1/\sqrt{2})\,(1, 0, \pm 1, 0)^T\,\delta_{n,m} \tag{3.9}$$

where m refers to the input cell number

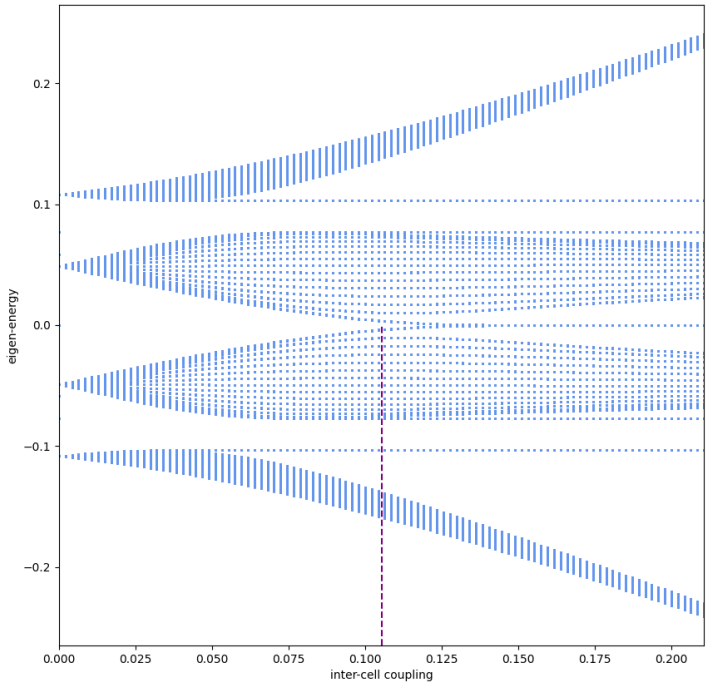

Figure 3.2.1: **Energy spectrum E of the Superlattice as a function of the inter-cell coupling strength**
The middle gaps are separate when $\tau < \tau_0$, closing and reopening at τ_0 (topological transition point), and divorcing since $\tau > \tau_0$.

In our simulation, we choose the mid $8th$ cell in 15 cells, so the initial state is:

$$a_8 = (1/\sqrt{2})\,(1, 0, \pm 1, 0)^T \tag{3.10}$$

Recalling the equation of the spectral amplitudes $C_l(k)$ and the displacement $\mathcal{D}_z$:

$$\begin{aligned} C_l(k) &= (1/2\pi) \sum_n \langle u_l(k) \mid a_n(0) \rangle \exp(-ikn) \\ 2\pi \sum_l \int_{-\pi}^{\pi} dk\, |C_l(k)|^2 &= 1 \\ \mathcal{D}(z) &= (1/z) \int_0^z d\xi \sum_{n=-\infty}^{\infty} n \langle a_n(\xi) \mid a_n(\xi) \rangle \end{aligned} \tag{3.11}$$

We then depict the light intensity evolution patterns in the left panels of fig 3.2.3, and the displacements of trivial/non-trivial cases in the right panels. It is interesting that the non-trivial case with a inter-cell coupling strength $\tau > \tau_0$ has a more ”localized”

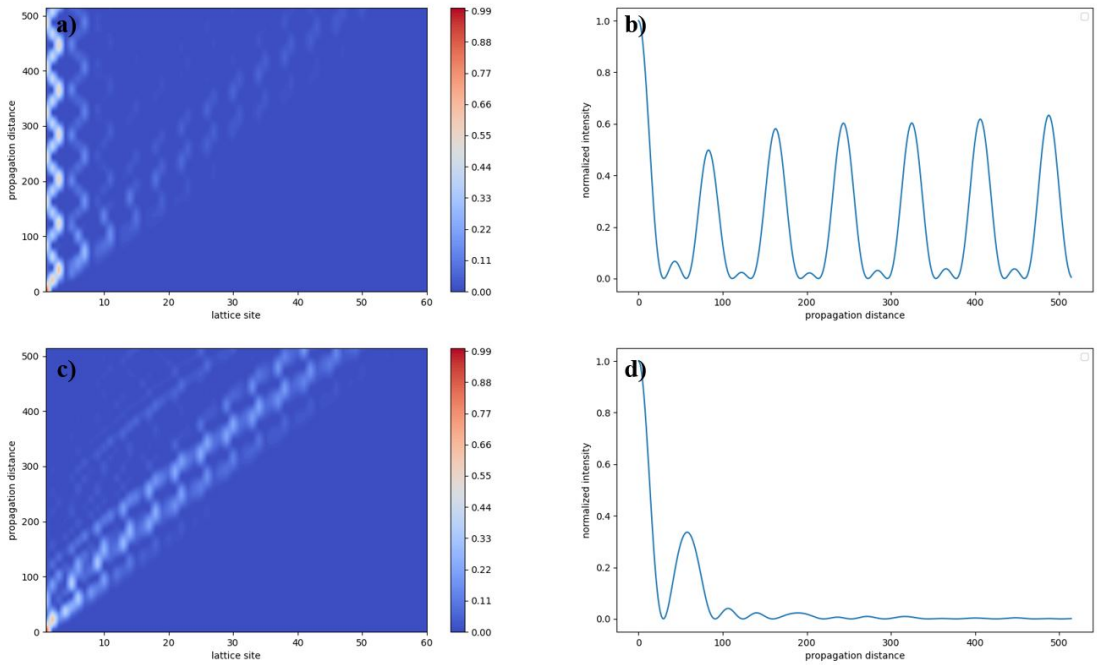

Figure 3.2.2:
a),c) refer to the topological nontrivial superlattice; b),d) refer to the topological trivial superlattice a),c)Numerically-simulated beam intensity evolution along normalized propagation distance for left-edge excitation. b),d) The oscillation of the light intensity in the edge waveguide.

beam, which is well visualized. The simulation result for the displacements is 0 for $t_1 < \tau_0$ and -0.25 for $t_2 > \tau_0$. τ_0 is the gap closing point where the topological transition occurs. This exciting method using the displacement measurement enables us to probe the topological Zak phase directly.

In real experiment, it is important to decide a sample rate of a single device, and we must be care about the efficiency and the accuracy at the same time. We pre-design a $300\mu m$ length device in fig 3.2.4, and set the sampling points at five distances: $(40, 80, 120, 160, 200)\ \mu m$. The left panel shows the rough simulation patterns for the five sampling points we choose.

In the right panel, it is clear that for the upper trivial case, the displacement approaches 0; for the lower non-trivial case, the displacement approaches -0.25, which is the same as the theoretical prediction. Now this simulation link the topological Zak phase with five directly sampling measurements for the light intensity in certain distances. It is a strong connection between the recondite concept and a intuitive physical quantity.

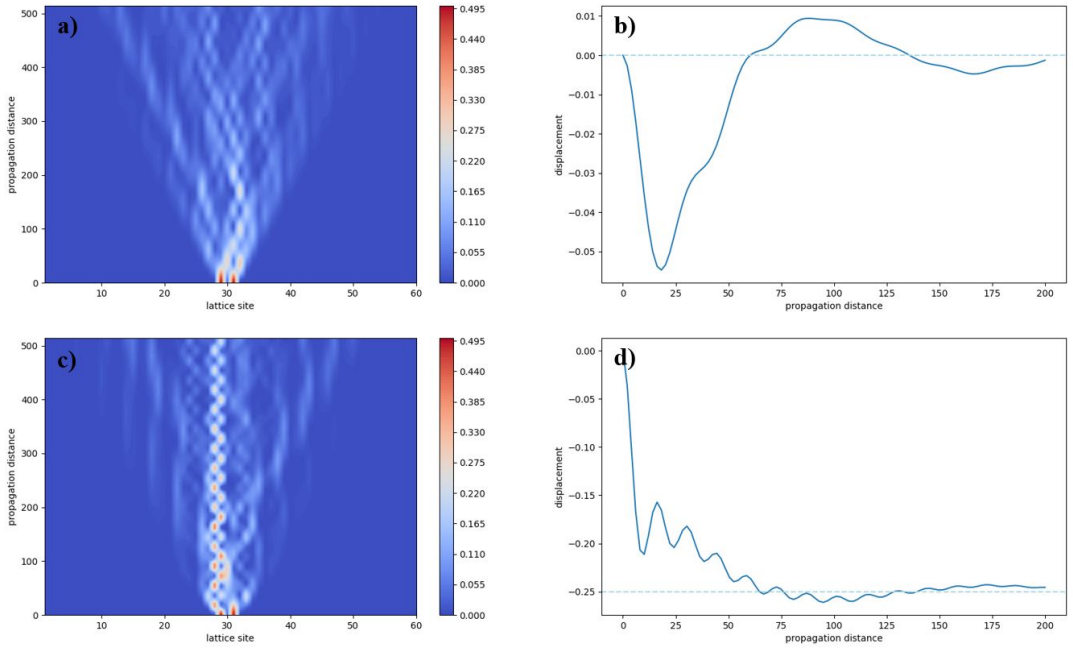

Figure 3.2.3:
a),c)Numerically-computed beam intensity evolution along normalized propagation distance for bulk excitation

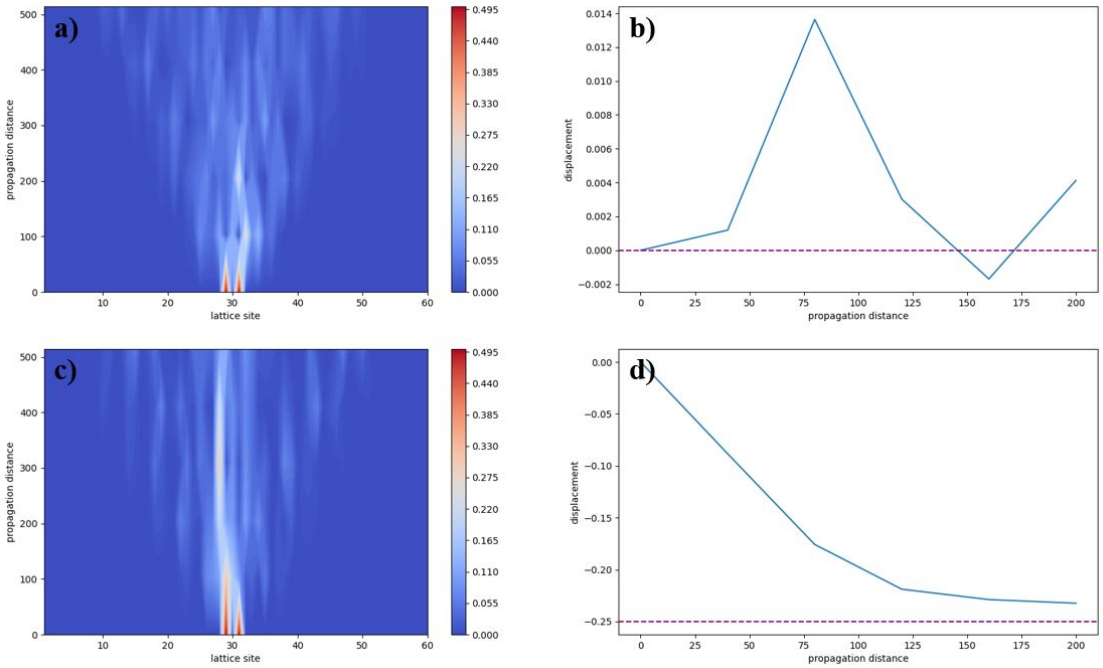

Figure 3.2.4: **Simulation results with 5 sampling points (40,80,120,160,200)** μm b) and d) shows clearly that with these 5 sampling distances, the displacement $D(z)$ still approaches 0 and -0.25 respectively, which means our design is reasonable.

Chapter 4

Sample Fabrication

In this chapter we present how we fabricate the chips. The main technology involved is the e-beam system installed in the cleanroom provided by the Albanova Nanolab. Our topological photonic chips for probing the Anderson phase and the Zak phase are based on the commercial Si wafers. These wafers are covered with 3.3 μm SiO_2 as the substrate and 250 nm Si_3N_4 as the waveguide layer.

4.1 Lithography

Lithography is a technique to fabricate a chip based on the CAD design. The process is performed through illuminating a light-sensitive photomask (resist) on the top of the sample. After the exposure, we can remove away parts of the exposed photo-resist film. There are two main resist in lithography technique: The positive resist and the negative resist. The positive resist means that we washed off the designed pattern of the photomask after exposing, when the negative resist refers to washed off the unexposed pattern. The following schematic drawn by Hesam Shahali[19] illustrates this concept well. In this project we focus on the negative resist technique and fabricate the protruding waveguides array on a chip.

The Rayleigh criterion indicates that the angular resolution is proportional to wavelength:

$$\theta \approx 1.22\frac{\lambda}{D} \tag{4.1}$$

To get a better resolution and fabricate the structure in nano scale, we choose electron beam lithography (EBL) system rather than traditional optical lithography. The

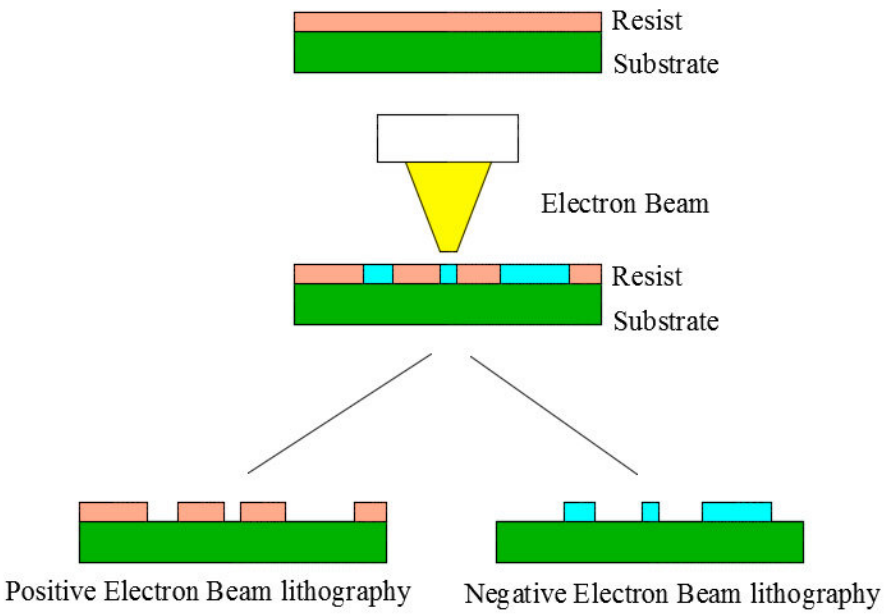

Figure 4.1.1: **The principle of Electron beam lithography.**

following figure shows the EBL system we use. The beam control system can only move in a limited range, so the sample is divided into several writing fields. After finishing one field, we move the sample stage and work into the next field. However, the writing field area of EBL system is small compared with the optical lithography due to the decrease of the beam wavelength. It is important to carefully design the lattice part of the chips within one writing field. The reason is stitching errors in waveguides, which occur when the ebeam stage moves between different fields. These small gaps in the waveguides can not be neglected, as they have similar scales to the coupling distances of the waveguides. Fig 4.1.2 shows the Raith Voyager EBL system in Albanova NanoFab lab.[20]

4.2 Etching

After Lithography, the substrate is etched to form the waveuides. In this project we use reactive ion etching. Our aim is to transfer a designed pattern to an nano-scale structure accurately. The fig 4.2.1 published by Anton Möller[21] illustrates the mechanism of the selectivity and isotropy in etching. The selectivity manifests the ability of etching the sample in a chosen depth. An etching technique with high selectivity would only etch the pre-planned film layer and stop, while a technique with low selectivity would over etch and sputter some underlying materials. The isotropy manifests the ability of etching the sample in a chosen direction. An anisotropic etching

Figure 4.1.2: **The picture of the Raith Voyager EBL System in Albanova NanoFab lab.**

technique can etch the film in a vertical direction without affecting the lateral materials, while an isotropic technique would etch in all directions which results in a non-vertical sides.

To achieve both anisotropy etching, we use a CF_4 based plasma with the Oxford Plasmalab 100 system shown in fig4.2.2[22]. We generate the CF_4 plasma in a low-temperature near-vaccum setting and bombard the sample to knock off the areas without the protection of the etch-resistant resist remaining from the lithography process.

The following fig 4.2.3 [23]shows the principle of Inductively Coupled Plasma Reactive Ion Etching. We send a RF signal into a coil to generate a high-density plasma and control the plasma ion concentration by controlling the RF signal. The plasma is then injected into a separated chamber. The sample after the lithography process is placed in a stage applied with another RF source. By controlling the second RF signal we apply a negative voltage in the sample and accelerate the ions vertically. The ions bombard the top surface of the sample and sputter the unwanted parts.

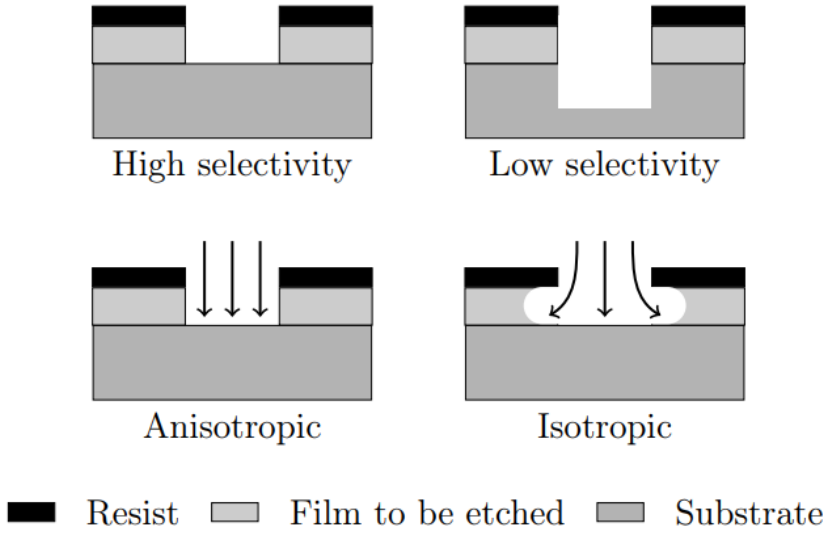

Figure 4.2.1: **The schematic of the selectivity and the isotropy for etching process**

Figure 4.2.2: **The picture of Oxford plasmalab 100 system**

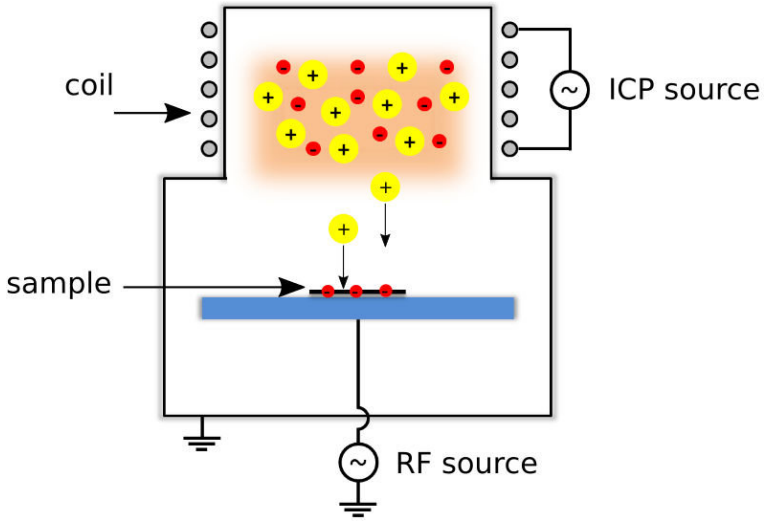

Figure 4.2.3: **A schematic of ICP-RIE instrument**

4.3 Cladding

For the photonic circuits to probe the Zak phase in the superlattice, we add a top cladding layer. The cladding we choose in this project is polymethyl methacrylate(PMMA). Adding this layer has two functions: 1. Give a better protection for the circuits on the chip. 2. Enable symmetric mode in vertical direction in (Si_3N_4), as the refractive index of PMMA is very close to the bottom oxide layer. Here we present a schematic of the pmma cladding around the silicon nitride waveguides in fig 4.3.1.

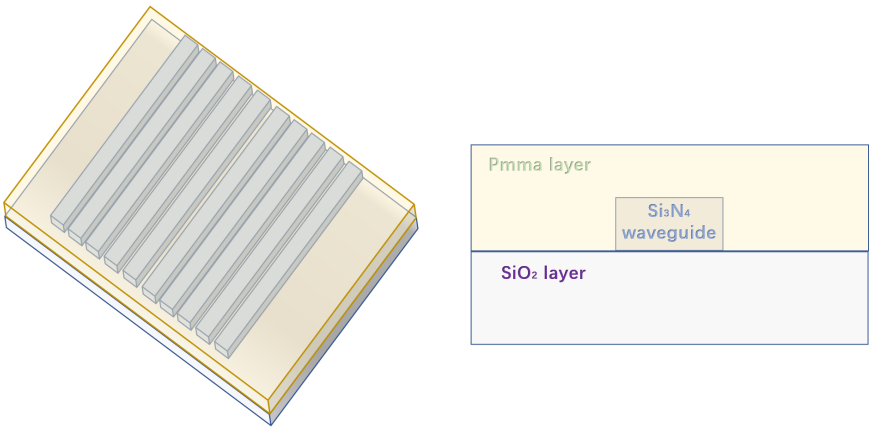

Figure 4.3.1: **A schematic of the PMMA cladding**

4.4 Chips

Here we present several images of the on-chip topological photonic lattices structure, taken using a scanning electron microscope (SEM) in fig 4.4.1 :

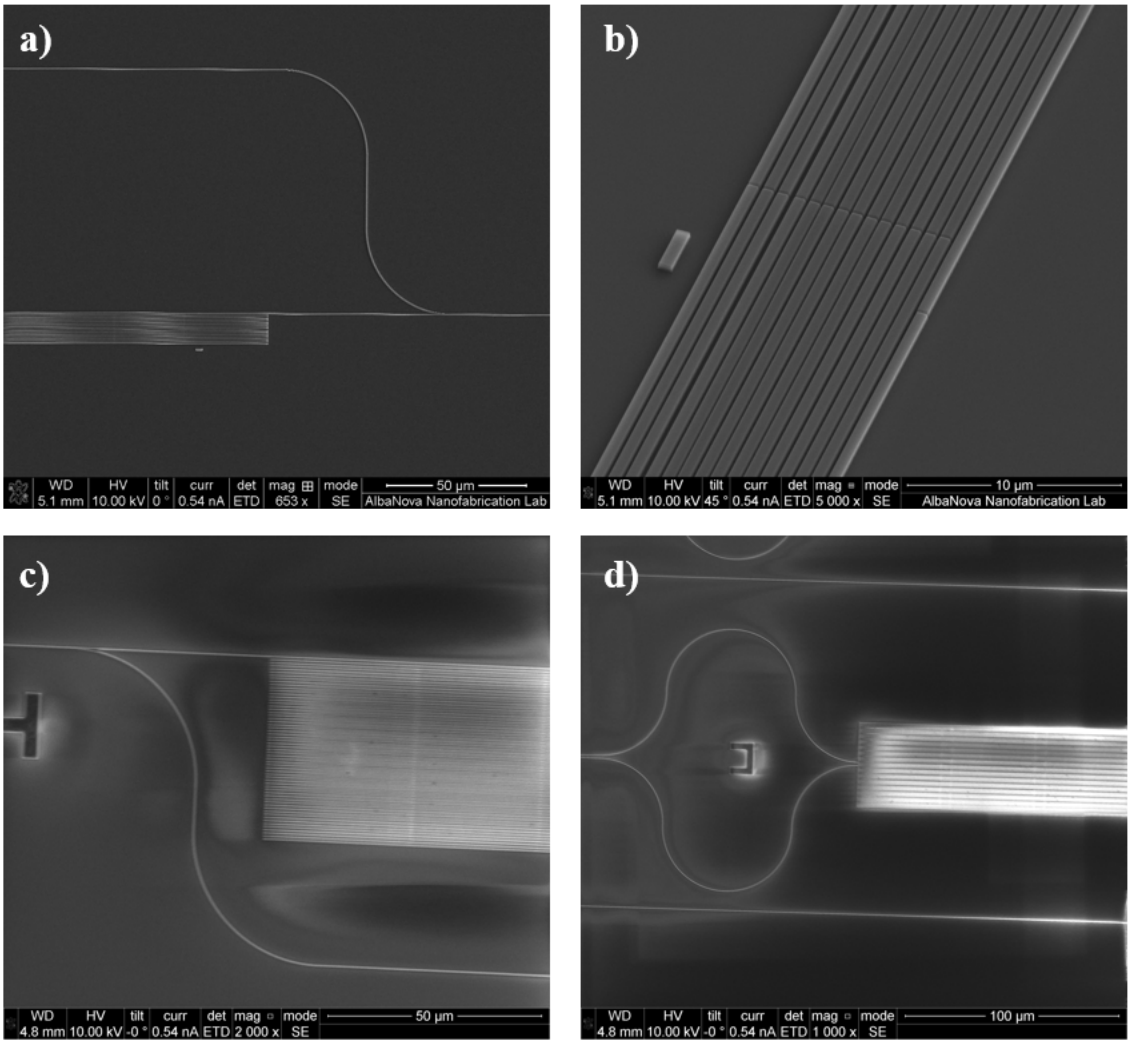

Figure 4.4.1: **SEM pictures** a) the SSH lattice with one monitor waveguide. b) SSH lattice with 15 waveguides and the loss induced scattering approach (LISA) structure. c) edge excitation structure with one monitor waveguide for superlattice. d) bulk excitation structure with one monitor waveguide for superlattice.

Chapter 5

Experimental Setup

In this chapter we introduce the experimental methods and the setup we used to perform the experiment. We simulated the coupling strength between the waveguides versus waveguide separation as show fig 5.0.1. This relation allows us to transfer the coupling strengths in the theritical models to physical gaps between the waveguides. All the simulation and measurement are based on the transverse electric (TE) mode.

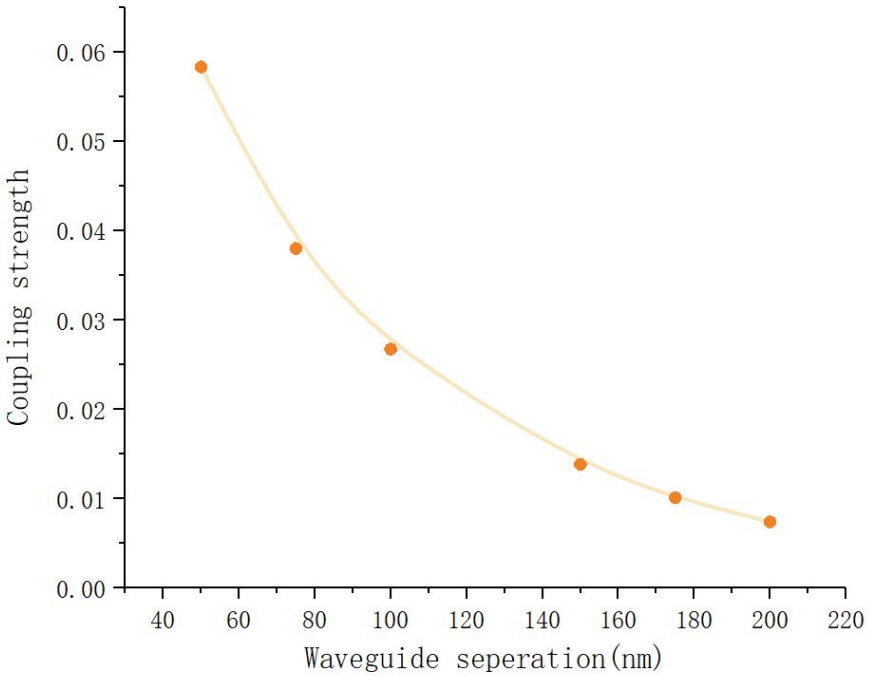

Figure 5.0.1: **Coupling strength /μm between two waveguides versus separation distance**

After fabrication, we mount the chip on a holder and place it on a 5-axis stage, which enables us to adjust the position of the chip. The schematic of the experiment set is shown in fig 5.0.2. We use a 795nm toptica coherent laser to excite the topological photonic lattice. The light is coupled out with a (polarization maintain)PM fiber to a 3-paddle polarization controller. In the output arm there is a PBS which only transmits the TE mode. The output beam is collimated with a 100X objective and focus on the detector. By tuning the polarization controller and monitoring the detector to get maximum counts, we can selectively excite the photonic lattice with TE mode. We top-image evolution pattern of the light along the propagation distance with a 50X objective (Mitutoyo Apochromatic NIR Objectives,MY50X-825) and a charge-coupled device (CCD) camera.

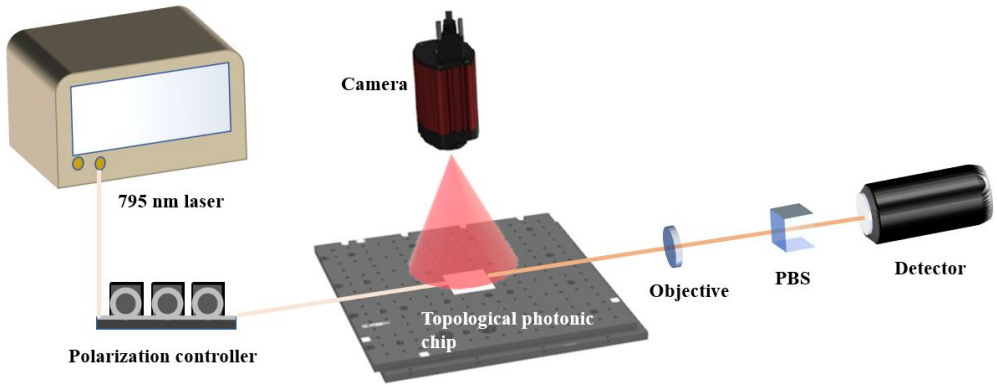

Figure 5.0.2: **Schematic of the experiment setup** The source generates a continuous wave 795 nm laser, and we use a polarization controller to excite the fundamental TE mode for the chip. We collect the light emitted from the induced scattering sites in top image with a microscope system with a CCD camera.

It is worth noting that the size of the waveguides and the separations are in hundred-nanometer scale, which is below the Abbe diffraction limitation calculated below:

$$d = \frac{\lambda}{2n \sin\theta} = \frac{\lambda}{2\mathrm{NA}} \tag{5.1}$$

where the NA means the numerical aperture. The MY50X-825 has a NA=0.42,the coherent laser source centered at 795 nm, which means the diffraction limitation is:

$$d = \frac{795\ \text{nm}}{2\text{NA}} = 946.4\ \text{nm} \tag{5.2}$$

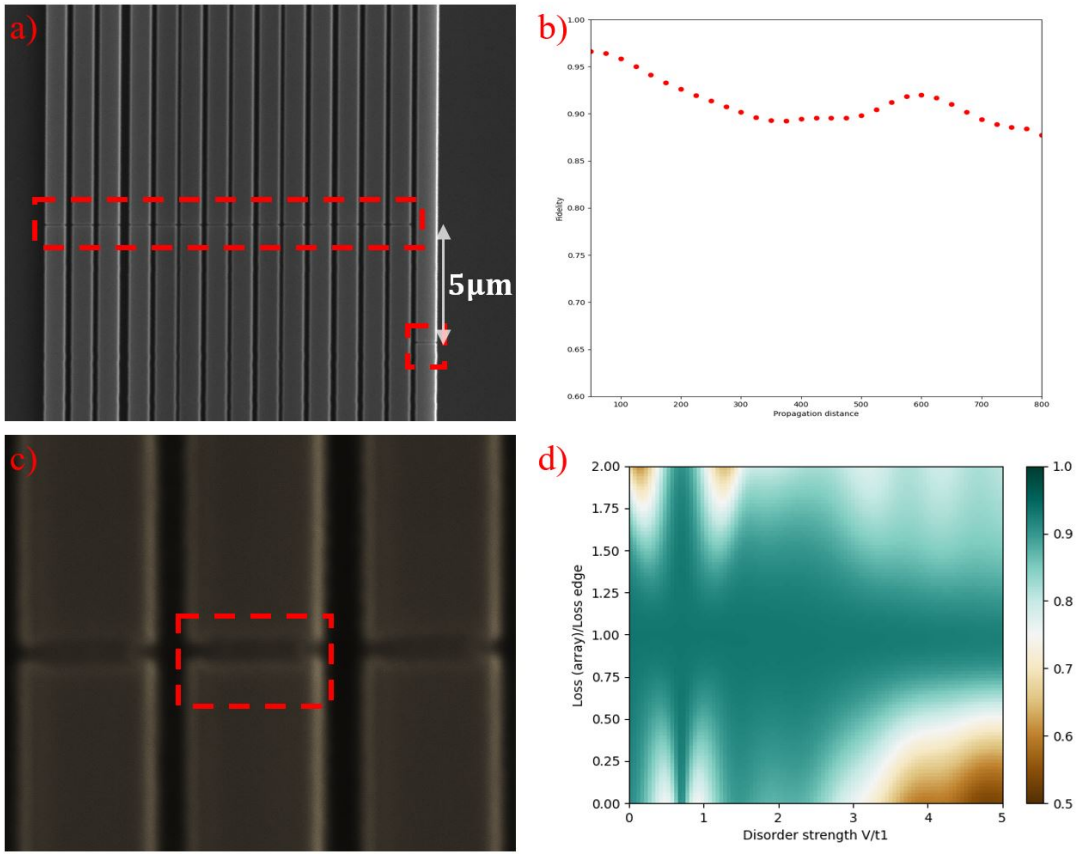

Figure 5.0.3: **LISA structure and fidelity** a) SEM image for gap in edge waveguide, and the gaps of the remaining waveguides to keep uniform loss. c) Magnified SEM image of deliberately introduced gap. b) The fidelity of edge waveguide along the light propagation direction d) Two dimensional plot of the state fidelity after 800 μm propagation for different disorder strength and the ratio between the edge loss and the array loss.

The diffraction limitation reaches a thousand-nanometer scale, so distinguishing different waveguides in a nanosized array is beyond the resolution of a modern optical microscope, result in the difficulty of image the evolution of the light intensity in the edge waveguide. To overcome this challenge, we developed a new method that facilitate monitoring the nano-scale light dynamics with a loss induced scattering approach (LISA). We deliberately introduce a series of tiny gaps in the excitation waveguide, and retrieve the light amplitudes by measuring the intensity of light scattered in these gaps. The simulated results show that the light dynamic would still keep high fidelity after these gaps. The fidelity is defined as the inner product of the lossless state with the loss induced state:

$$Fidelity = \frac{\langle \vec{a_{lossless}}, \vec{a_{loss}} \rangle}{\|\vec{a_{lossless}}\| \cdot \|\vec{a_{loss}}\|} \tag{5.3}$$

We also make uniform loss (array loss) in the remaining waveguides after 5 μm from the excited site to compensate the loss in the edge waveguide (edge loss). The structure and the fidelity are shown in fig 5.0.3.

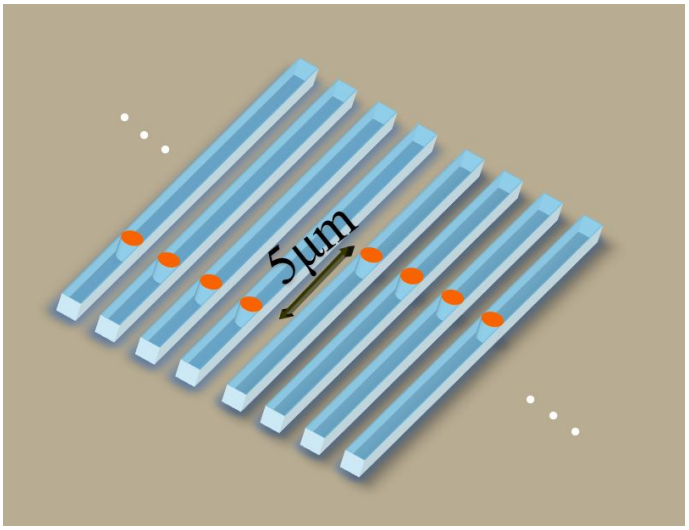

Figure 5.0.4: **Odd even columns LISA structure for superlattice**

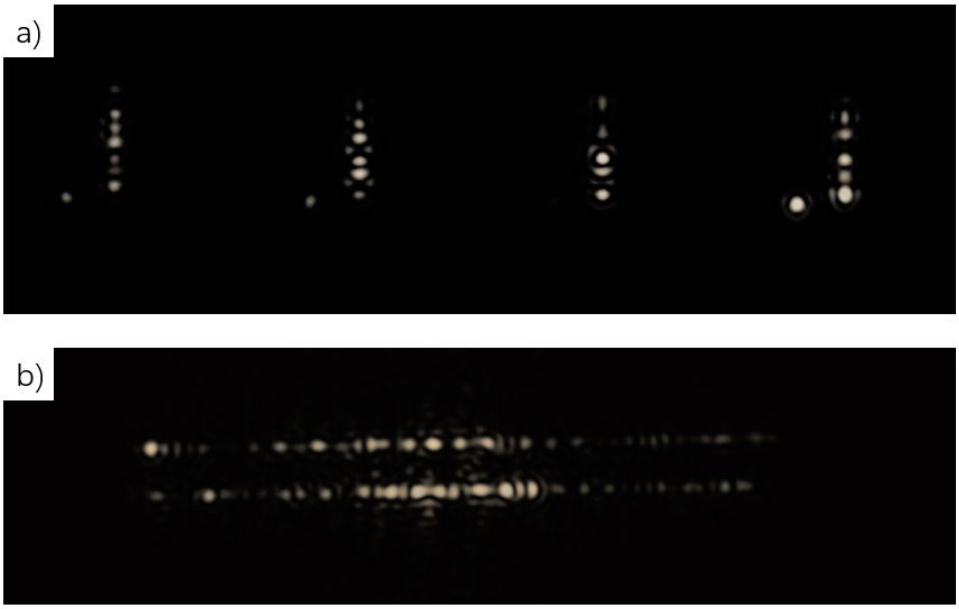

Figure 5.0.5: **Top images** a) Top image of excited SSH lattice b) Top image of excited superlattice

After fine calibration, we excite the photonic lattice, then we turn the micrometers of the 5-axis stage to maximize the excitation power and move the LISA structure into the

field of view of CCD camera. We take picture and then move along the light propagation direction (z) to take the next picture. In superlattice, there are 60 sites far more than 15 sites in SSH lattice, so we also introduce a two column LISA structure to separate the odd and even cells in fig 5.0.4.

We present the typical pictures of LISA structure in disordered SSH lattice and topological superlattice in fig 5.0.5. Fig.5.0.5 a) shows the top image of the light intensity distribution in the excited topological SSH lattices. The spots in the bottom are the light scattered from the edge waveguide, while the upper array of spots are the light scattered from the remaining waveguides. Fig.5.0.5 b) shows the top image of the light intensity in the excited topological superlattice at a certain distance. The top spots are the light scattered from the even number cells (4 waveguides in a cell), the bottom spots are the light scattered from the odd even number cells.

After acquiring the images, we run scipy.signal.find peaks module in python and can get the plot of the intensity distribution along the propagation distance z.

Chapter 6

Data Analysis

6.1 Topological Anderson phase

To calculate the correlation function and probe the topological Anderson phase, we need to retrieve both the amplitude and the phase information. In the part of retrieving the amplitude, we use the OpenCV module in python and read the image as a grayscale matrix.

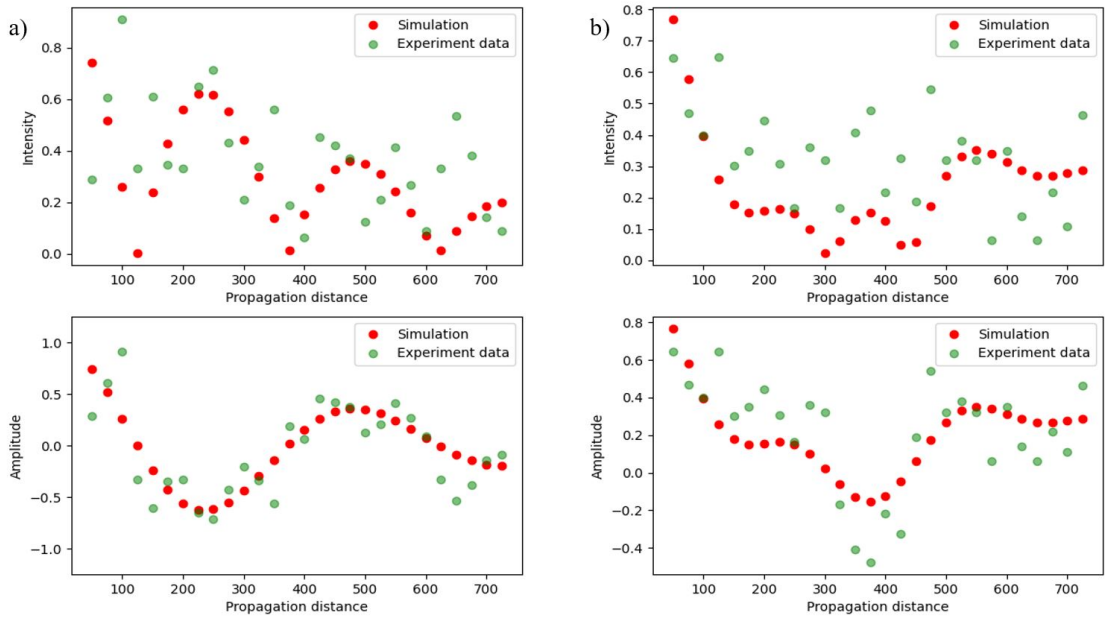

Figure 6.1.1: **Intensity extraction and Amplitude reconstruction versus propagation distance** a) Disorder strength V=1.0t_1 b) Disorder strength V=2.5t_1

Then we use scipy.signal.find peaks module to trace the intensity information for every single gap along the propagation distance, where the sampling period is 25μm. By

squaring the intensity, we get the amplitude information in two disordered SSH lattice with disorder strength $V_1 = 1.0t_1$ and disorder strength $V_2 = 2.5t_1$. It is worth noting now all the amplitudes only have positive signs.

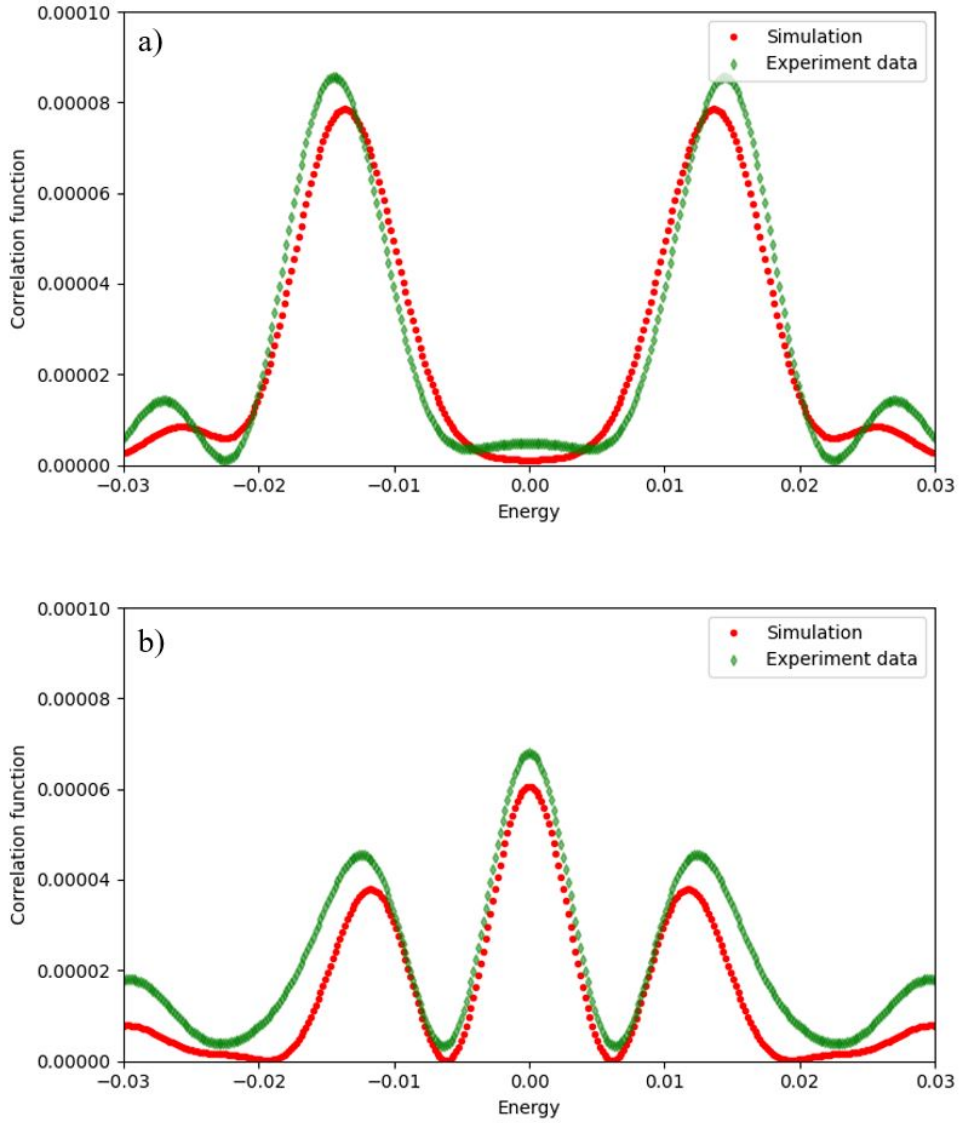

Figure 6.1.2: **Correlation function versus Energy** a) Disorder strength V=1.0t_1 b) Disorder strength V=2.5t_1

However, the phase information lost is needed to calculate the correlation function but lost in an intensity-based CCD image, so we can not retrieve the phase information simply. The most decisive step is to decide the sign (± 1) of the amplitude. The change of this sign is due to the boundary reflection of the light in the lattice. We extract the discrete points and find the local minimum points of them. In every local minimum points, the sign flips from $+1(-1)$ to $-1(+1)$. By multiply the sign into the amplitude we traced before, we can get both the amplitude and phase information which is shown

in fig 6.1.1. The energy spectrum is also depicted in fig 6.1.2 by applying the theorem of correlation function we mentioned before:

$$C(E) = \frac{1}{L}\int_0^L dz a_1(z)\exp(iEz) \tag{6.1}$$

6.2 Topological Zak phase

6.2.1 Edge excitation

We firstly try the edge excitation. We excite the edge waveguide and monitor the light intensity evolution in it.

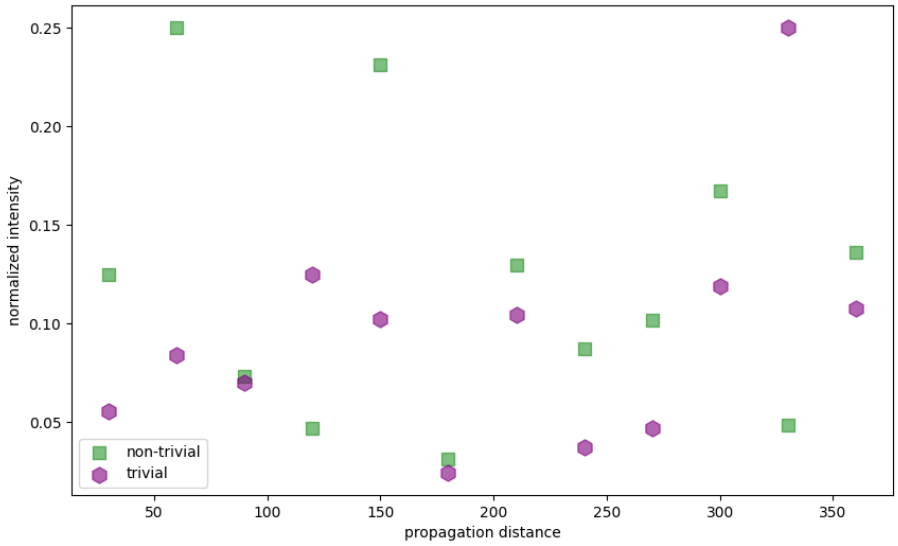

Figure 6.2.1: **Intensity oscillation** Although the trivial and non-trivial case have different topological Zak phase 0 and π, it is challenging to distinguish them.

However, according to what we emphasized before, both trivial and non-trivial Zak phase would have localization on the edge and result in obvious oscillation, so it would be hard to identify these two conditions if the inter-cell coupling strength τ is not so far away from the critical point $\tau = t_1 t_3/t_2$. We use the same intensity retrieval technique in 6.1. The intensity oscillation is shown in fig 6.2.1.

6.2.2 Bulk excitation

Then we turn to the bulk excitation, where we excite the superlattice in the first and third waveguide in the middle cell. The displacement is defined as:

$$\mathcal{D}(z) = (1/z) \int_0^z d\xi \sum_{n=-\infty}^{\infty} n \langle a_n(\xi) \mid a_n(\xi) \rangle \tag{6.2}$$

In our chip, we have 15 cells and take five sampling points z_i at 40, 80, 120, 160 and 200 μm, so the displacement has the discrete form:

$$\mathcal{D}_i(z) = (1/z) \sum_{k=1}^{i} \frac{\sum_{n=-7}^{7} n \langle a_n(z_i) \mid a_n(z_i) \rangle}{\sum_{n=-7}^{7} \langle a_n(z_i) \mid a_n(z_i) \rangle} \tag{6.3}$$

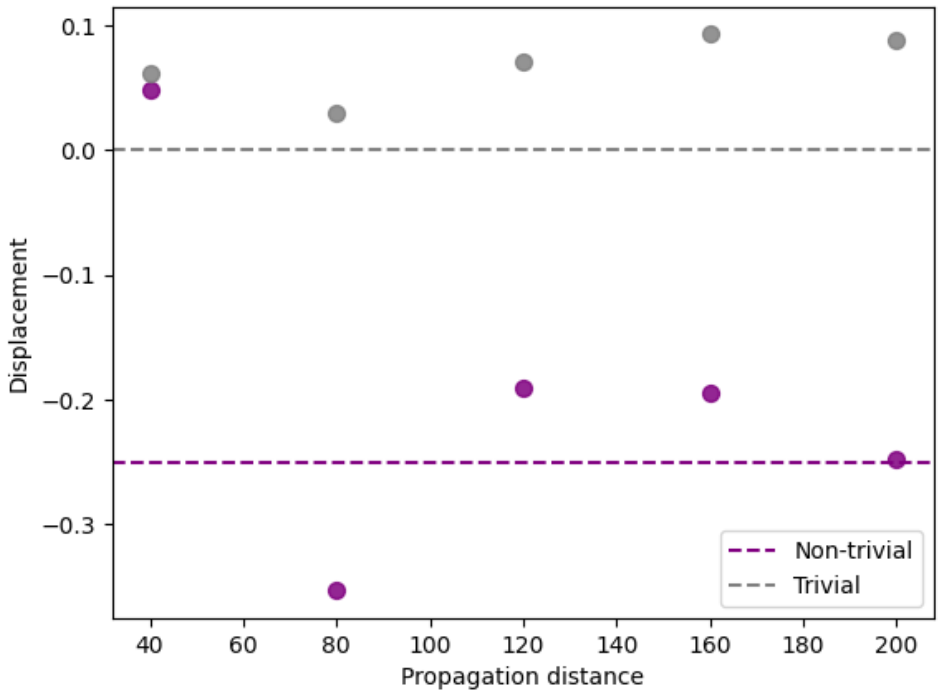

Figure 6.2.2: **Displacement of trivial and non-trivial superlattice versus propagation distance** The displacement of trivial lattice ($\tau_1 = 0.052$) is depicted by grey marker, which converges on 0; the displacement of non-trivial lattice ($\tau_2 = 0.194$) is depicted by purple marker, which converges on -0.25.

where i is the refers to the i-th sampling point, z refers to the propagation distance, and we define the number of the cell in range of (-7,+7) from left to right. Then we draw the displacement of light in superlattice with trivial and non-trivial Zak phase in

fig 6.2.2. The results match our theoretical prediction, where trivial case refers to 0 displacement and 0 Zak phase; non-trivial case refers to -0.25 displacement and π Zak phase.

Chapter 7

Conclusion and Future outlook

7.1 Conclusion

The degree project is divided into two parts: Probing the topological Anderson phase transition in disordered SSH lattice and probing the Zak phase in superlattice.

In the first part, we successfully reconstruct the correlation function spectrum C_E and observe the Anderson phase transition. In SSH lattice with disorder strength $V < 2.0t_1$, we observed trivial topological phase; in SSH lattice with disorder strength $V > 2.0t_1$, we observed non-trivial topological phase $Q = 1$, which means there is a topological transition in the critical point $V = 2.0t_1$. We also successfully proposed the loss induced scattering approach (LISA) method to probe the intensity information of waveguide at nano-scale.

In the second part, we study both the edge and bulk excitation methods of probing Zak phase. We proved that edge waveguide excitation method is not able to accurately probe the Zak phase in two superlattice with different inter-cell coupling strength. Then we perform the bulk excitation experiment, and successfully retrieve the beam displacement and reconstruct the Zak phase in two superlattice with different inter-cell coupling strength above or below the critical point $\tau = t_1 t_3/t_2$.

7.2 Future Work

We investigate the influence on the displacement for different phase shifts of the light in the third waveguide. Now the initial state of the mid 8th cell (15 cells in total)

reads:

$$a_8 = (1/\sqrt{2})(1, 0, e^{i\theta}, 0)^T \tag{7.1}$$

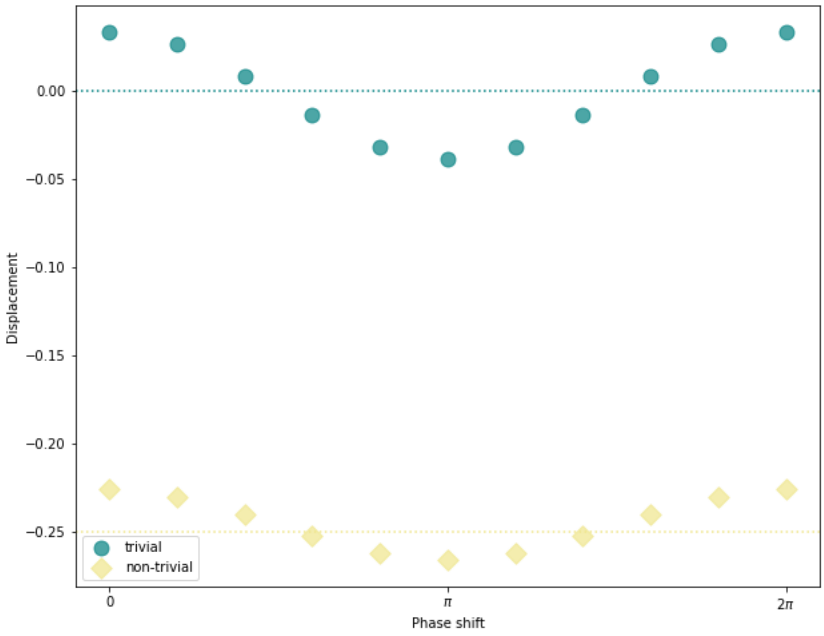

Figure 7.2.1: **Displacement versus phase shift of the third site excitation**

Then we simulate the light propagation and draw the relationship between displacement and phase shift in fig 7.2.2. The plot shows an oscillation. So here rise the question: Could we probe the Zak phase using bulk excitation method with different phase shift? How to realize the phase shift between two inputs?

We would use a heater in one arm of the Y-splitter to control the phase shift of the light coupled to the third site. The optical path length is defined as:

$$\text{OPL} = \int_C n \, \mathrm{d}s \tag{7.2}$$

The refractive index of the waveguide material as as we heat the arm and change the optical path length. The Thermo-optic coefficient of silicon nitride (SiN) is measured in [24].

We assume that our working temperature range with this heater to be (20,60) °C, the thermo-optic Y-splitter structure is shown in fig 7.2.4

We also plan to explore the behaviour of asymmetrical thermo-optic Y-splitter.

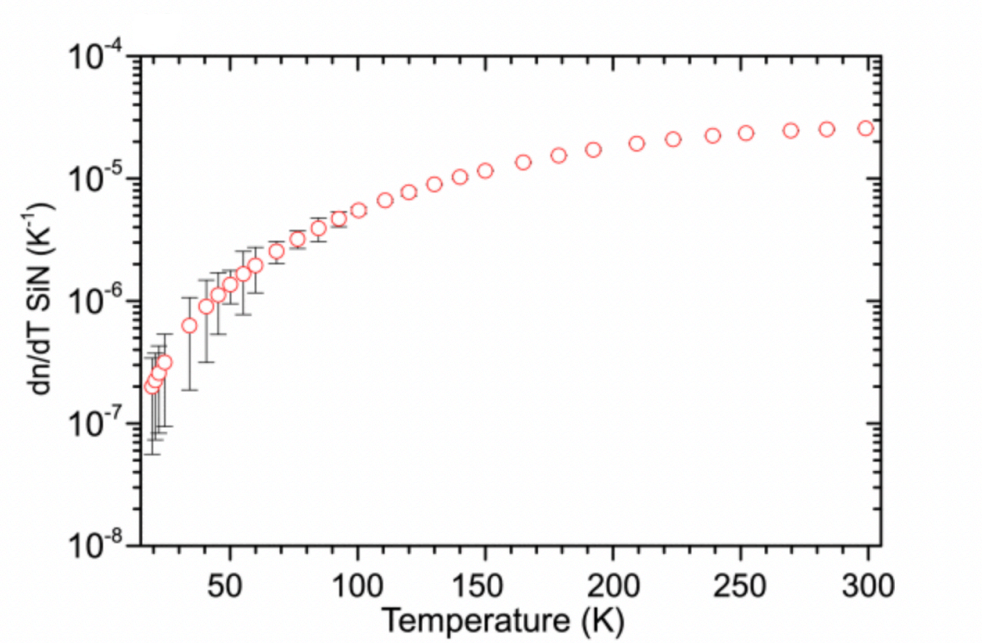

Figure 7.2.2: **Thermo-optic coefficient of SiN** [24]

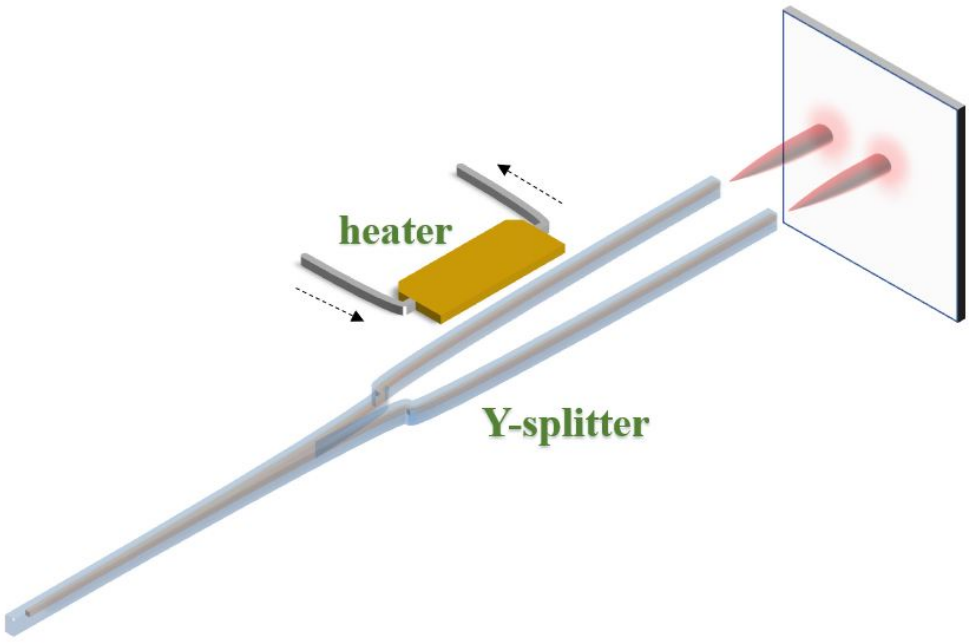

Figure 7.2.3: **Schematic of thermo-optic Y-splitter**

We draw the schematic of this structure and simulate the output intensity versus the temperature and the asymmetric length ΔL in a Mach-Zehnder interferometer (MZI):

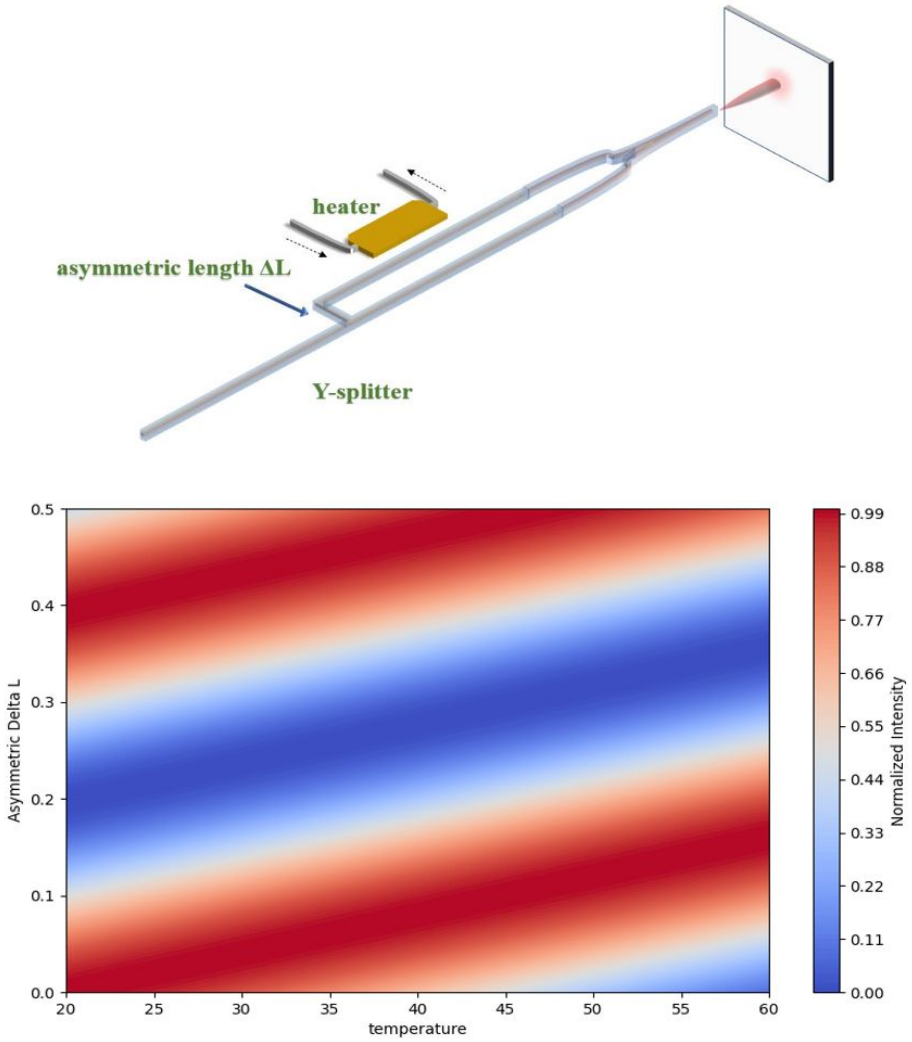

Figure 7.2.4: **Schematic of asymmetric thermo-optic Y-splitter and the intensity profile**

The next step we will fabricate a thermo-optic MZI to accurately measure the parameters, and design the phase control for superlattice bulk excitation accordingly.

Bibliography

[1] Klitzing, K. v., Dorda, G., and Pepper, M. “New Method for High-Accuracy Determination of the Fine-Structure Constant Based on Quantized Hall Resistance”. In: *Phys. Rev. Lett.* 45 (6 Aug. 1980), pp. 494–497. DOI: 10.1103/PhysRevLett.45.494. URL: https://link.aps.org/doi/10.1103/PhysRevLett.45.494.

[2] Haldane, F. D. M. and Raghu, S. “Possible Realization of Directional Optical Waveguides in Photonic Crystals with Broken Time-Reversal Symmetry”. In: *Phys. Rev. Lett.* 100 (1 Jan. 2008), p. 013904. DOI: 10.1103/PhysRevLett.100.013904. URL: https://link.aps.org/doi/10.1103/PhysRevLett.100.013904.

[3] Wang, Zheng, Chong, Yidong, Joannopoulos, John D, and Soljačić, Marin. “Observation of unidirectional backscattering-immune topological electromagnetic states”. In: *Nature* 461.7265 (2009), pp. 772–775.

[4] Nayak, Chetan, Simon, Steven H, Stern, Ady, Freedman, Michael, and Sarma, Sankar Das. “Non-Abelian anyons and topological quantum computation”. In: *Reviews of Modern Physics* 80.3 (2008), p. 1083.

[5] Zhou, Xin, Wang, You, Leykam, Daniel, and Chong, Yi Dong. “Optical isolation with nonlinear topological photonics”. In: *New Journal of Physics* 19.9 (2017), p. 095002.

[6] Segev, Mordechai and Bandres, Miguel A. “Topological photonics: Where do we go from here?” In: *Nanophotonics* 10.1 (2021), pp. 425–434.

[7] Lagendijk, Aart, Van Tiggelen, Bart, and Wiersma, Diederik S. “Fifty years of Anderson localization”. In: *Phys. Today* 62.8 (2009), pp. 24–29.

[8] Schwartz, Tal, Bartal, Guy, Fishman, Shmuel, and Segev, Mordechai. “Transport and Anderson localization in disordered two-dimensional photonic lattices”. In: *Nature* 446.7131 (2007), pp. 52–55.

[9] Song, Juntao, Liu, Haiwen, Jiang, Hua, Sun, Qing-feng, and Xie, X. C. "Dependence of topological Anderson insulator on the type of disorder". In: *Phys. Rev. B* 85 (19 May 2012), p. 195125. DOI: 10.1103/PhysRevB.85.195125. URL: https://link.aps.org/doi/10.1103/PhysRevB.85.195125.

[10] Johansson, CH and Linde, JO. "Röntgenographische Bestimmung der Atomanordnung in den Mischkristallreihen Au□ Cu und Pd□ Cu". In: *Annalen der Physik* 383.21 (1925), pp. 439–460.

[11] Longhi, Stefano. "Probing topological phases in waveguide superlattices". In: *Optics letters* 44.10 (2019), pp. 2530–2533.

[12] Zak, J. "Berry's phase for energy bands in solids". In: *Physical review letters* 62.23 (1989), p. 2747.

[13] Kivelson, S. "Wannier functions in one-dimensional disordered systems: Application to fractionally charged solitons". In: *Phys. Rev. B* 26 (8 Oct. 1982), pp. 4269–4277. DOI: 10.1103/PhysRevB.26.4269. URL: https://link.aps.org/doi/10.1103/PhysRevB.26.4269.

[14] Zeuner, Julia M, Rechtsman, Mikael C, Plotnik, Yonatan, Lumer, Yaakov, Nolte, Stefan, Rudner, Mark S, Segev, Mordechai, and Szameit, Alexander. "Observation of a topological transition in the bulk of a non-Hermitian system". In: *Physical review letters* 115.4 (2015), p. 040402.

[15] Fulga, I. C., Hassler, F., Akhmerov, A. R., and Beenakker, C. W. J. "Scattering formula for the topological quantum number of a disordered multimode wire". In: *Phys. Rev. B* 83 (15 Apr. 2011), p. 155429. DOI: 10.1103/PhysRevB.83.155429. URL: https://link.aps.org/doi/10.1103/PhysRevB.83.155429.

[16] Corrielli, G., Della Valle, G., Crespi, A., Osellame, R., and Longhi, S. "Observation of Surface States with Algebraic Localization". In: *Phys. Rev. Lett.* 111 (22 Nov. 2013), p. 220403. DOI: 10.1103/PhysRevLett.111.220403. URL: https://link.aps.org/doi/10.1103/PhysRevLett.111.220403.

[17] Feit, M.D, Fleck, J.A, and Steiger, A. "Solution of the Schrödinger equation by a spectral method". In: *Journal of Computational Physics* 47.3 (1982), pp. 412–433. ISSN: 0021-9991. DOI: https://doi.org/10.1016/0021-9991(82)90091-2. URL: https://www.sciencedirect.com/science/article/pii/0021999182900912.

[18] Cardano, Filippo, D'Errico, Alessio, Dauphin, Alexandre, Maffei, Maria, Piccirillo, Bruno, Lisio, Corrado de, De Filippis, Giulio, Cataudella, Vittorio, Santamato, Enrico, Marrucci, Lorenzo, et al. "Detection of Zak phases and topological invariants in a chiral quantum walk of twisted photons". In: *Nature communications* 8.1 (2017), pp. 1–7.

[19] Shahali, Hesam, Hasan, Jafar, Wang, Hongxia, Tesfamichael, Tuquabo, Yan, Cheng, and Yarlagadda, Prasad. "Evaluation of Particle Beam Lithography for Fabrication of Metallic Nano-structures". In: *Procedia Manufacturing* 30 (Jan. 2019), pp. 261–267. DOI: 10.1016/j.promfg.2019.02.038.

[20] Liljeborg, Anders. *Raith Voyager EBL System*. URL: https://www.nanophys.kth.se/nanolab/voyager/voyager.html.

[21] Möller, Anton. *Piezoelectric tuning of integrated photonic delay circuits*. 2019.

[22] Liljeborg, Anders. *Oxford Plasmalab 100*. URL: https://www.nanophys.kth.se/nanolab/rie-cryo/webman/man.html.

[23] Gili, Valerio Flavio. "All-dielectric nonlinear nanophotonics". PhD thesis. Nov. 2018.

[24] Elshaari, Ali W., Zadeh, Iman Esmaeil, Jöns, Klaus D., and Zwiller, Val. "Thermo-Optic Characterization of Silicon Nitride Resonators for Cryogenic Photonic Circuits". In: *IEEE Photonics Journal* 8.3 (2016), pp. 1–9. DOI: 10.1109/JPHOT.2016.2561622.